NOTE TO USERS

UNIVERSITÉ DE MONTRÉAL

ANALYSIS AND DESIGN OF SUBSTRATE INTEGRATED WAVEGUIDE CAVITY FILTER FOR MICROWAVE & MILLIMETER WAVE APPLICATIONS

HOU WENXIN

DÉPARTEMENT DE GÉNIE ÉLECTRIQUE
ÉCOLE POLYTECHNIQUE DE MONTRÉAL

MÉMOIRE PRÉSENTÉ EN VUE DE L'OBTENTION
DU DIPLÔME DE MAÎTRISE ÈS SCIENCES APPLIQUÉES
(GÉNIE ÉLECTRIQUE)
AVRIL 2005

Your file Votre référence
ISBN: 0-494-01340-0
Our file Notre référence
ISBN: 0-494-01340-0

UNIVERSITÉ DE MONTRÉAL

ÉCOLE POLYTECHNIQUE DE MONTRÉAL

Ce mémoire intitulé:

ANALYSIS AND DESIGN OF SUBSTRATE INTEGRATED WAVEGUIDE CAVITY FILTER FOR MICROWAVE & MILLIMETER WAVE APPLICATIONS

présenté par : Hou Wenxin

en vue de l'obtention du diplôme de : Maîtrise ès sciences appliquées

a été dûment accepté par le jury d'examen constitué de :

M. Akyel Cevdet, D.Sc.A., président

M. Wu Ke, Ph. D., membre et directeur de recherche

M. Bourry Mathieu, Ph. D., membre

DEDICATION

To my parents, and
Xiaochun and Haoran for their love and support

ACKNOWLEDGEMENTS

I would like to express my deepest gratitude to my director, Dr. Ke Wu, for giving me the chance to pursue my master studying, for his support, and his guidance during this project research period. I would like to thanks as well to Mr. Uwe Rosenberg for many helpful suggestions.

I would give my thanks to Mr. Jules Gauthier and Mr. Roch Brassard for their technical assistance, Mr. René Archambault for his software support, and Mr. Marsan Eric for his support on measurement.

I would also like to thank to Mr. Dominic Deslandes, Mr. Ping Yang, Mr. Taijun Liu, Mr. Xidong Wu, Mr. Xiaoma Jiang and Mr. Feng Xu for many helpful discussions and suggestions and to all the researchers at POLY-GRAMES.

A special thanks is also extended to Mr. Ramdan Aissani, Mr. Thomas Sieverding and their company AdvanSys Electronix for their generous software trial supplying.

Finally I would like to extend my gratitude to my husband, my son and to my parents and sisters for their endless love and support in spirit.

ABSTRACT

The purpose of this research project is to design and develop a substrate integrated waveguide (SIW) cavity band-pass filter with pseudo elliptic function response.

SIW is a technique which can integrate planar circuits and waveguide on the same substrate by using metallized grooves (slots) or metallized via holes on the substrate. This technique features low cost and compact size.

To design a narrow-band coupled cavity filter, the fundamental step is to create the synthesis platform of coupling matrix. In this work, an advanced analytical gradient-based optimization technique has been used for the coupling matrix synthesis.

In the SIW design scheme, a planar waveguide cavity coupling (H-plane) topology was considered and deployed, therefore, an innovative coupling method based on the use of cavity transformation properties with a compact configuration of TE_{102}/TE_{201} mode cavities has been used. This flexible coupling scheme permits the design of a topology with the filter input and output placed on the same side, which further decreases the overall structure size. Our precision laser cutting technology guarantees excellent mechanical tolerances as well as tuning-free fabrication, and ceramic material was adopted to meet the processing hardness requirement.

A commercial software package HFSS was used to simulate the initial physical

dimensions of resonance cavities and coupling slots, and it was also used to achieve the design tuning process. An efficient tuning method has been developed and used in this work, and its technical features have been verified in the design of a symmetric structure narrow-band filter, but difficulties were encountered in dealing with asymmetric structure cross-coupled high-order filter. Finally, a mode-matching technique based optimization process has been used for the asymmetric cross-coupling structure, which was shown to be a much more powerful and appropriate technique in the design of complex and tuning-free filter.

In addition, transition from microstrip line to SIW was designed to facilitate the measurements. Our measurements under different thermal conditions were performed using a HP-8510 network analyzer and a temperature test chamber. It has been verified that our synthesis, simulation and measurement results are in excellent agreement.

RÉSUMÉ

Le but de ce projet de recherche est de développer et de construire un filtre passe-bande avec une cavité en guide d'onde intégré sur substrat (SIW).

Le SIW est une technique qui peut intégrer les circuits planaires et les guides d'ondes sur le même substrat par des sillons métallisés ou par l'intermédiaire des trous métallisés, cela donne de bas prix et une taille compacte.

Pour la conception le filtre à bande étroite ayant un couplage de cavité, l'étape fondamentale est la synthèse de la matrice de couplage. Dans ce travail, une technique d'optimisation analytique avancée basé sur la méthode du gradient est utilisée pour la synthèse de la matrice de couplage.

Dons cette structure d'une topologie à couplage de cavité de guide d'onde planaires (Plan-H) est proposée, c'est une méthode de couplage innovatrice basée sur l'utilisation des propriétés de transformation de cavité utilisant une configuration compacte de cavités de mode TE_{102}/TE_{201} est donc utilisée. Cette structure de couplage flexible permet une topologie avec l'entrée et la sortie sur le même côté, ce qui diminue corridérablement la taille de la structure complète. La technologie de coupure précise au laser garantit des tolérances mécaniques excellentes aussi bien que la libre variation de conception. Le matériau choisi permet de céramique satisfaire à l'exigence de dureté

dans le procédé de fabrication.

Le progiciel commercial HFSS a été utilisé pour simuler les dimensions physiques initiales des cavités de résonance et des fentes couplées, aussi il a été utilisé pour complété le processus de conception de réglage. Une méthode de réglage efficace a été développé, utilisé et vérifiée dans la conception de structures de filtre a bande étroite symétrique, mais des difficultés ont été rencontrées sur la structure asymétrique du filtre d'ordre supérieur et couplé. Finalement le processus d'optimisation basé sur la technique d'adaptation de mode a été utilisé pour la structure asymétrique de filtre d'ordre supérieur et couplé, ce qui s'est avéré être une technique puissante et très appropriée dans la conception complexe de filtre à sans réglage.

De plus, la transition de la ligne de microruban à SIW a été conçue pour faciliter les mesures. Nos mesures dans des conditions différentes de températures sont exécutées en utilisant l'analyseur de réseau HP 8510 et une Chambre de test en Température. Il a donc finalement été vérifié que la synthèse, la simulation et la mesure étaient en excellent accord.

CONDENSÉ EN FRANÇAIS
ANALYSE ET CONCEPTION DES FILTRES A GUIDES D'ONDES INTÉGRÉ SUR SUBSTRAT POUR APPLICATIONS À MICRO-ONDES ET ONDES MILLIMÈTRIQUES

Les Performances des systèmes de communication modernes dépendent essentiellement des caractéristiques des filtres, tels que une haute sélectivité et la compréhension de la bande de rejection de un ou plusieurs pôles aux fréquences limites (connus comme les zéros de transmission à bande d'arrêt), que l'on peut accomplir avec les filtres Chebyshev généralisés ou avec les filtres pseudo elliptique [24]. Concernant l'application à haute fréquence avec un facteur qualité Q élevé, ce type de filtre est généralement réalisé par des cavités de résonance de guide d'ondes directement couplées avec une ou plusieurs couplage de travers entre des cavités non adjacentes pour mettre en oeuvre les zéros de transmission de la bande d'arrêt. Les développements récents dans les MICs (Circuits Micro-ondes Intégré) et les MMICs (Circuits Micro-ondes Intégré Monolithique) indiquent le besoin de guide d'ondes intégrés sur substrat (SIW) qui peuvent être intégrés à la ligne de microruban ou sur d'autre circuits planaires sur le même substrat, cela donne des avantages d'obtention de bas prix et une taille compacte

au circuits. Cette étude se divise en quatre chapitres pour illustrer en détail comment un filtre, de fonction passe bande à 5 pôles, à cavité de résonance en SIW ayant une réponse a fonction pseudo elliptique est conçu et fabriqué. Ici une description concise du contenu des quatre chapitres sera présentée dans les quatre sections suivantes.

0.1. Synthèse et analyse du filtre à fonction pseudo elliptique

Ce filtre à réponse pseudo elliptique est préféré dans ce projet pour fonctionner à une fréquence centrale de 24GHz, avec une largeur de bande de 3 %, c'est-à-dire, 720MHz et deux zéros de transmission (TZs) seront accomplis symétriquement sur chaque côté de la bande passante, soit à 22.7GHz et 25.3GHz respectivement. Basé sur les spécifications ci-dessus, un calcul est exécuté en utilisant de formule (1.4.2) qui résulte du fait que le filtre d'ordre 5 doit rencontrer toutes ces exigences.

Les techniques de guides d'onde de sillons métallisés, synthétisés sur du substrat sont utilisées ici pour construire les cavités de résonance SIW. En raison de son épaisseur très mince, les points de structures SIW a la technique de fabrication qui permet le design direct de la cavité planaires (guide d'onde plan-H) couplé de façon direct, une méthode de couplage basée sur la combinaison des couplages de l'iris magnétiques et sur les propriétés de transformation TE_{10n}/TE_{n01} des modes des cavités planaires proposée par Uwe Rosenberg [3] est donc choisie dans notre conceptions de

filtre SIW.

Une configuration de filtre planaire à quatre pôles explique l'utilisation du principe des propriétés de transformation de mode TE_{10n}/TE_{n01} des cavités, présenté dans la Figure 1-4. On peut voir que bien que les champs magnétiques de la cavité exposent des composantes égales près magnétiques de l'iris, la direction des champs change de 180 degrés à la moitié de longueurs d'onde du couplage ce que l'on peut considérer comme un transformateur avec un ratio de -1, qui est approprié pour tous couplages principaux du filtre. Les distributions des champs magnétiques principales dans les cavités résultent des couplages principaux (M_{i1}, M_{12}, M_{23}, M_{34}, M_{4o}), il y a la possibilité de deux emplacements de l'iris différents pour le couplage principal M_{23}, en raison de l'arrangement du mode de cavité résonnante TE_{102} représentant le deuxième circuit de résonance (R2) et le mode de cavité résonant TE_{101} pour le troisième circuit de résonance (R3). Les emplacements sont définis aux deux moitiés de longueur d'ondes du mode de résonance TE_{102}. De là, le choix de l'emplacement de l'iris détermine la direction des champs électromagnétiques des cavités de résonances utilisables, c'est la direction du champ de mode TE_{101} de cavités représentant les circuits de filtre R3 et R4. De plus l'inverseur d'impédance combiné au couplage M_{23} est dans chaque cas négatif indépendamment de la position de l'iris, il n'y a cependant aucun changement dans le chemin de couplage principal du filtre.

Par ailleurs, la direction des champs de mode TE_{101} dans la cavité R4 détermine le signe de couplage magnétique M_{14} entre des cavités R1 et R4. Ainsi, le signe de M_{14} peut être transformé indirectement par la cavité de mode TE_{102} en combinaison avec l'emplacement du couplage de l'iris M_{23} pour la réalisation de caractéristiques de filtre arbitraires, c'est une fonction elliptique ou une réponse de phase linéaire. Pour une réalisation de fonction elliptique, les trois couplages doivent avoir le même sens et le dernier couplage restant de sens opposé. L'arrangement de couplages de notre filtre à 5 pôles à fonction pseudo elliptique peut alors être établi par tous les couplages principaux qui sont pour être avec l'un positif et un couplage croisé non adjacent entre le 2ème et les 5ème cavités pour être un négatif pour réaliser le bande d'arrêt TZs, la topologie est présenté dans la Figure 1-6.

La matrice de couplage de fréquence variable a été largement utilisée dans la synthèse de filtre passe-bande à résonateur couplés transverses. Selon la détermination ci-dessus de l'arrangement de couplage, une matrice de couplage peut être construite dans la forme de (1.5.11). Un certain nombre de chercheurs ont suis du point beaucoup de sortes de méthodes sur la synthèse de matrice de couplages, par exemple, en extrayant le pôle, par les transformations de similitudes et par une série de techniques d'optimisation [7] - [19]. En comparant toutes ces méthodes existantes, une technique d'optimisation à base de gradient analytique proposée par Smain [19] a été préférée pour

être adopté dans ce projet a cause de ses avantages de haute efficacité et par la capacité de programmation.

On explique l'information détaillée dans la section 1.5 sur le mise en place de la fonction de coût et son modèle de base et à propos de l'exécution de la procédure d'optimisation. Un code de MATLAB basé sur cette méthode est présenté dans l'annexe, utilise la matrice de couplage et les résistances d'entrée et de sortie R_1 et R_2 peuvent être réalisées comme indiqué dans (1.5.12). Les réponses désirables sont illustrées dans la Figure 1-7.

0.2. Réalisation physique du filtre de fonction pseudo elliptique à 5 pôles

Dans le chapitre 2, on explique comment les dimensions physiques initiales de cavités de résonance et des fentes de couplages sont calculées, simulées et basées sur les résultats de synthèse du chapitre 1 et une liberté de conception de post réglage ou un processus d'optimisation doivent être exécutés.

Tout d'abord une sorte de matériel de substrat doit être choisi afin de débuter la conception de cavités de résonance. Considérant les pré requis de technologie de fabrication disponible dans notre centre de recherches, la compétence des techniciens contrôlant le nouveau processus de fabrication, une céramique de haute dureté et

d'épaisseur très mince est suggéré. Les performances de certains paramètres de matériaux sont présentées dans la Tableau 2-1.

Parce que le mode de propagation dominant étant utilisé est ici le mode TE_{10}, de la formule (2.2.1) on peut voir que, sa constante de propagation β de mode TE_{10} est seulement reliée à la largeur "a" en raison de m=1, n=0. Donc, la hauteur ou l'épaisseur "b" dans la direction y, comme indiqué dans la Figure 2-1, peuvent être choisis par des dimensions arbitraires sans impact sur la propagation de mode TE_{10}, permettant ainsi son intégration dans un substrat mince. Comme cela est démontré dans la Tableau 2-1, l'épaisseur SIW ou la hauteur "b" a été fixée à 10 mil, la procédure subséquente de procéder est de déterminer la largeur "a" et la longueur "l" de la cavité de résonance rectangulaire SIW. Au guide d'ondes rectangulaire, le premier pré requis, pour définir les dimensions de section croisées, est de garantir que seulement le mode de propagation dominant TE_{10} sera propagé. La Figure 2-3 nous donne une distribution graphique de modes distinguées, sur lequel on peut voir que le principe de choix des dimensions du guide d'ondes croisé pourrait être faites par l'inégalité (2.3.7) et (2.3.10).

Pour la fréquence d'opération de 24GHz, la longueur d'onde est $\lambda = {}^{c}/_{f} = 492.1mil$, référant à la dimension du type standard de guide d'ondes WR-42 rempli d'air, qui a un "a" ayant 420mil, ainsi pour le SIW avec permittivité relative $\varepsilon_r = 9.9$ (vu de la Tableau 2-1), les paramètres devrait être modifié comme

$a = 420/\sqrt{\varepsilon_r} = 133.5mil$, $\lambda = 492.1/\sqrt{\varepsilon_r} = 156.4mil$. Comme il a été démontré dans le Chapitre 1, le mode TE_{102} sera utilisé comme le mode résonant dominant. De la formule (2.3.8), il peut être observé que, pour le mode TE_{10}, sa longueur d'ondes de coupure est $\lambda_c = 2a = 267mil$. Alors, sa longueur d'ondes, le guide d'ondes devrait être calculée comme $\lambda_g = 193mil$. Pour le mode résonant TE_{102}, la longueur de cavité résonante rectangulaire "*l*" devrait être équivalente à deux nombre d'onde stationnaire, c'est-à-dire, $l = \lambda_g$.

Pour conclure, la cavité de résonance rectangulaire SIW est conçue en sélectionnant la largeur a=133.5 mil, la hauteur b=10 mil, la longueur *l*=193 mil.

La performance de filtre et son niveau de perte d'insertion sont énormément influencés par le facteur de qualité déchargé, Q_u. Q_u est un paramètre de spécification qui pointe vers la sélectivité de fréquence des systèmes à micro-ondes résonant ainsi qu'à la relation entre le stockage d'énergie et les pertes dans le résonateur. Sa définition est exprimée dans la formule (2.4.1). Sur la base des formules (2.4.2) à (2.4.4), Q_u pourrait être ainsi obtenu comme $Q_u = 522$. Qui pourrait aussi être vérifiée dans le progiciel commercial ANSOFT, en utilisant sa solution de mode propre, Q_u peut être obtenue $Q_u = 517$. Il est observé que ces deux Q_u sont presque les mêmes. On montre une autre expression pour Q_u dans la formule (2.4.5), duquel on peut voir que Q_u qui est approximativement dans la proportion directe au volume de cavité V, dans la proportion

inverse à la cavité à l'intérieur de la superficie S et la profondeur de peau δ. Donc, pour réaliser une haute valeur de Q, on devrait considérer une valeur plus haute de V/S. Pour cette conception de filtre à 5 pôles, augmentation Q doit nécessité augmentation de l'épaisseur de substrat "*b*", qui augmente la complication et la tolérance de machinerie pendant le processus de fabrication, on n'aura besoin de faire quelques efforts et plus d'expériences afin d'obtenir des solutions futures.

La perte d'insertion en bande complète dont (IL) du filtre passe-bande peut être grossièrement évalué par la formule (2.4.6), de laquelle une valeur évaluée de $IL = 1.4dB$ peut être obtenue. En réalité, la perte supplémentaire sera causée par la transition d'entrée et sortie avec la ligne de micro ruban, la radiation dépend aussi de beaucoup du processus de métallisation, ainsi on pourrait s'attendre à la valeur un peu plus haute d'IL en pratique. Les effets de dissipation peuvent être représentés en remplaçant simplement la variable de fréquence $j\Omega$ pour le circuit sans perte par $(j\Omega + d)$ pour inclure les pertes, ou $d = 1/wQ_u$. Réévaluez les paramètres de dispersion S_{11} et la réponse S_{21} par cette substitution en utilisant la méthode de synthèse décrite dans le Chapitre 1, la courbe de réponse attendue pourrait être réalisée comme indiqué dans la Figure 2-4. Il est démontré que dû à une valeur plus petite de Q, une plus haute perte d'insertion en bande est rencontrée comme analysé ci-dessus et le rejet TZs ne peut pas être aussi pointu comme cela a été démontré dans la Figure 1-8. Cependant,

les performances générales comme indiqué dans la Tableau 1-1 peuvent être accompli, cela signifie que le facteur de qualité Q peut satisfaire les pré requis pour mettre en oeuvre notre filtre de fonction pseudo elliptique.

La Figure 2-5 montre des éléments localisés dérivés de réseau à deux ports de filtre passe bande. Un arrangement consistant à une alternance en séries et parallèle de résonateurs est plutôt difficile à réaliser dans des circuits à micro-ondes, c'est une approche tout à fait pratique de remplacer les circuits parallèles résonants du filtre passe-bande par des inverseurs d'impédance ou d'impédance inversant des transformateurs comme indiqué dans la Figure 2-6. La définition et la propriété d'un inverseur d'impédance sont exprimées par la formule (2.5.1) et (2.5.3). Dans notre cas, les fentes de couplage parmi les cavités de résonance de guide d'ondes agissent comme des inverseurs d'impédance. Commençant par les coefficients de couplage normalisés M_{ij} et les résistances l'entrée et sortie R_1 et R_2 qui ont été réalisé dans le Chapitre 1, nous les transférons d'abord en coefficients de couplage dénormalisés k_{ij} en utilisant la formule (2.5.7), on calcule ensuite les valeurs d'inverseur d'impédance normalisées K_{ij} par la formule (2.5.8), finalement, les paramètres de dispersion de chaque structure de couplage peuvent être calculés en appliquant la formule (2.5.2). Adhérez aux paramètres de dispersion désirables, en faisant des simulations dans le progiciel commercial HFSS, les dimensions initiales de toutes les cavités et les fentes de

couplages peuvent être obtenus comme démontré dans la formule (2.5.10).

La Figure 2-10 donne les réponses de paramètre de dispersion simulées en appliquant les dimensions initiales, on peut dire que la perte de retour en bande est seulement autour de -10dB, le côté juste TZ n'apparaît pas significativement, une méthode de réglage efficace doit donc être appliqué. Jan et Kjetil [23] ont suggéré une procédure de réglage pour des filtres de guide d'ondes symétriques avec des couplages croisés dans le plan E. Nous essayons cette méthode innovatrice pour notre structure de filtre SIW à couplage asymétrique dans le plan H avec une légère modification, les procédures de réglage sont décrites en détail dans la section 2.6. Après les efforts de réglage, une réponse améliorée est obtenue comme indiqué dans la Figure 2-15. Comparez la Figure 2-10 et la Figure 2-15, on peut voir qu'après le réglage, la réponse en bande obtient une grande amélioration et la réponse de bande d'arrêt s'améliore quant à elle, un tout petit peu. Cependant la réponse de bord de la bande passante ne fonctionne pas toujours bien, ce qui signifie que la largeur de bande d'ondulation égale est plus rétrécie que celle voulue. À partir des phénomènes observés ci-dessus, nous pouvons arriver à la conclusion que, pour le filtre de guide d'ondes symétrique à couplage croisé, cette méthode de réglage peut être très utile et efficace. Mais en ce qui a trait au couplage asymétrique croisé, l'interaction entre les couplages devient plus forte, compliquée et sensible. En outre, plus les zéros de transmission sont loin de la bande

passante, plus c'est difficile pour le côté inférieur et supérieur des zéros de transmission d'être symétrique, cela a été observé par nos simulations et également conclu en référence [24].

Par la suite, un processus d'optimisation global est inévitable pour la structure de filtre d'ordre supérieur asymétrique à couplage croisé afin de réaliser la libre conception post réglé. Une technique d'adaptation de mode basé sur un progiciel commercial *μWave* Wizard est alors faite. Basé sur le réglage des résultats (2.5.11), c'est un gain de temps dans le travail en utilisant *μWave* Wizard pour faire l'optimisation avec plus de dix-sept variables globales à optimiser en même temps. On montre un résultat d'optimisation convergé dans la Figure 2-16. Il peut être observé qu'après l'optimisation, une perte de retour en bande $A_{e\min} \geq 17dB$ est réalisée avec un accomplissement désiré de la largeur de bande de 3 %, de même que la performance de bande d'arrêt est réalisé par $A_{\min} \geq 70dB$ avec deux TZs sur les deux côtés respectivement. Les dimensions finales optimisées sont listées en (2.5.12).

0.3. Conception de la transition micro ruban

De manière à exécuter les mesures, une transition entre SIW et la micro ruban est nécessaire. Pour une épaisseur de substrat h=10 mil, une ligne micro ruban de $50\,\Omega$ doit être raisonnablement utilisée avec la largeur w=9.6 mil. La conception de la transition

commence par l'optimisation de la structure qui consiste en, des sections de ligne micro ruban connectée avec une ligne microbus 50 Ω et une section de SIW respectivement sur chaque côté, comme cela est montré dans la Figure 3-1. Le processus d'optimisation a été exécuté dans le simulateur HFSS en changeant la longueur "*l*" et la largeur "*d*" jusqu'à l'obtention d'un meilleur résultat. Avec la valeur de *l*=61 mil, d=37 mil, une perte d'insertion meilleur que -0.12 dB et une perte de retour moins que -25 dB dans la bande passante sont obtenues dans cette étape comme le démontre la Figure 3-2.

En raison de la disposition spéciale, l'entrée et la sortie sont sur le même côté de la structure, requise par la mesure, une section de courbure doit être impliquée dans la conception de transition. Entre la bougie fine et la ligne de micro ruban, insérez la section de courbures de 90°, comme indiqué dans la Figure 3-3. Fixez la taille de bougie fine par la valeur optimisée ci-dessus et fixez la longueur de la ligne de micro ruban à 160 mil, laissez le rayon de courbure "r" (le rayon central) à la variable d'optimisation. Finalement, une valeur de r=70mil donne un très bon résultat de la perte d'insertion meilleur que -0.03 dB et la perte de retour moins que -30dB dans la bande passante comme illustré dans la Figure 3-4.

Connectez la structure de transition avec le filtre SIW et prenez en considération tout l'ensemble, la perte diélectrique et la perte métallique, conduisez la simulation de nouveau dans HFSS pour vérifier si la conception de transition peut maintenir la

performance de filtre ou pas. Il donnera aussi des réponses complètes finales du filtre conçu. Les résultats sont exposés dans la Figure 3-5. Il peut être observé qu'en comparant la Figure 3-5a) avec la Figue 2-16, la perte de retour en bande garde sa bonne performance, cependant, en raison du facteur de qualité Q bas plus la perte de la transition du micro ruban, la perte d'insertion à la fréquence centrale 24.03 GHz serait augmentée à -3.615 dB. Pour améliorer la caractéristique de réponse d'insertion en bande, tel qu'analysé dans le Chapitre 2, nous pourrions essayer de faire plus d'expériences en utilisant des matériaux de substrat différents avec l'épaisseur différente. Tout cela dépend aussi beaucoup de l'accumulation des expériences de traitement et l'amélioration sur la technologie de traitement. Comparez les réponses à large bande dans la Figure 3-5c) avec ceux dans la Figure 2-17, on peut voir que la performance de bande d'arrêt ne peut pas être authentique à cause de la structure de transition micro ruban ouverte, cela limite l'application du filtre SIW à ceux qui n'exigent pas de rejet extrême dans la large bande d'arrêt, dit ci-dessous de -40dB.

0.4. Fabrication et mesures

Comme démontré dans le Chapitre 2, les sillons métallisées seront utilisées pour réaliser la cavité SIW. Pour continuer à garder la cavité toujours connecté avec le substrat après le coupage par la machinerie, quelques très petites taille de bandes de

connexion sont conçues au milieu du mur latéral ou au bord du mur large en considérant la résonance du mode TE102, cela ne donne aucune influence à la réponse de filtre, mais une très petite augmentation de la perte d'insertion, disons moins que 0.1dB comptant sur la simulation, ce qui est négligeable. La fabrication a été réalisé par la machine au laser de notre centre de recherches, on a estimé d'avance une tolérance attendue de $\pm 1 mil$ dans la conception de dimension, ensuite une précision finale de $\pm 0.5 mil$ pourrait être réalisée. Le produit achevé est présenté à la Figure 4-1.

L'analyseur de réseau HP 8510 a été utilisé pour effectuer les mesures du circuit; pour faire des mesures corrigées d'erreur dans des médias de transmission non coaxiaux, la méthode de calibrage TRL doit être utiliser. Cette technique de calibrage est basée sur une méthode " THRU-REFLECT-LINE ", comme décrite dans [25]. Une longueur non nul "THRU" est utilisée, mais spécifiée pour avoir un délai de zéro, le plan de référence sera établi au milieu du "THRU". La différence de longueur entre le "THRU" et le "LINE" doit être d'une longueur d'onde de $\frac{1}{4}$ ou 90 degrés de d'insertion phase au milieu de la porté de fréquence désiré. Cependant, la phase d'insertion de la longueur d'ondes $\frac{1}{4}$ du "LINE" variera avec la fréquence, à l'intérieur de la portée de fréquence, c'est-à-dire de la fréquence de début f_1 à la fréquence d'arrêt f_2, la différence de phase d'insertion entre le "THRU" et le "LINE" doit être comprise entre 20 et 160 degrés.

Après le calibrage TRL, mesuré sous la température ambiante, les réponses de

paramètre de dispersion sont obtenues comme présenté dans la Figure 4-3 et la Figure 4-4. De ces deux Figures, on peut observer que les réponses mesurées sont en accord avec celles simulées et le rejet de la bande d'arrêt pourrait être moins que -35 dB sur la gamme entière de largeur de bande de 50 %.

Mesurant à des conditions de températures différentes, on ressort la performance de fréquence de température de notre filtre de cavité SIW. Le phénomène de l'épaisseur de métallisation affecté à la perte d'insertion et à la performance fréquence température du filtre de cavité SIW est suggéré, ceci requiert des recherches substantielles dans le futur.

TABLE OF CONTENTS

TABLE OF FIGURES

TABLE OF TABLES

LIST OF SIGNS AND ABBREVIATION

FEM	Finite Element Method
IL	Insertion Loss
MIC	Microwave Integrated Circuit
MMIC	Monolithic Microwave Integrated Circuit
RL	Return Loss
SIW	Substrate Integrated Waveguide
TE	Transverse Electric
TM	Transverse Magnetic
TZ	Transmission Zero

INTRODUCTION

Performance of communication systems essentially depends on characteristics of filters such as high selectivity, and outstanding out-of-band rejections at finite frequencies (known as transmission zeros in stop band), which can be accomplished by a generalized Chebyshev filter or a pseudo elliptic filter [24]. Concerning the application at high frequency with high quality factor Q, this kind of filter is commonly realized by direct-coupled waveguide resonant cavities with one or more cross-couplings between non-adjacent cavities to implement the stop-band transmission zeros (TZs). Developments in the planar integration of microwave integrated circuit (MIC) and monolithic microwave integrated circuit (MMIC) have led to the invention of substrate integrated waveguide (SIW) which can be integrated with the microstrip line or other planar structures on the same substrate; this provides advantages of low cost and compact size. In Chapter 1 of this thesis, it will be illustrated in detail how an SIW cavity band-pass filter with pseudo elliptic function response is synthesized and analyzed.

To design a narrow-band coupled-cavity filter, the fundamental step is to create a synthesis procedure of coupling matrix. In this work, an analytical gradient-based optimization technique has been developed and used for the coupling matrix synthesis.

Main advantages of this synthesis technique are that it can synthesize filters of arbitrary even- or odd-orders with either symmetric or asymmetric responses; also its flexible programmability and rapid convergence make it a very efficient synthesis tool. A MATLAB code based on this method has been presented in Appendix.

In Chapter 2, it will be explained how the initial physical dimensions of resonant cavities and coupling slots are calculated and simulated on the basis of the synthesis results of Chapter 1. A software tuning procedure is described in detail to improve the filter performance. Also it will be demonstrated in which case an optimization process is inevitable to achieve a post-tuning free design.

A microstrip to SIW transition design will be made in Chapter 3 for the measurement purpose. Measurements under different thermal conditions will be presented in Chapter 4, and analysis results and comparison will be presented.

Finally, the whole project will be concluded and a set of future works will be proposed and discussed.

Chapter 1. SYNTHESIS AND ANALYSIS OF PSEUDO-ELLIPTIC FILTER

1.1. Objective

A millimeter-wave band-pass filter having pseudo-elliptic function response based on the substrate integrated waveguide (SIW) resonant cavity technique will be synthesized and analyzed. As a result of applying the SIW technique, a planar (H-plane) coupling scheme will be established by utilizing higher-order mode (overmoded) cavity transformation properties. Then, an analytical gradient-based optimization technique will be applied to the cross-coupled network synthesis.

1.2. Introduction of substrate integrated waveguide

Rectangular waveguide resonator has found a wide range of applications in microwave and millimeter-wave filter design due to its much higher Q factors, but it also suffers from the requirement of complex transition to integrated planar circuits. Therefore, this conventional technology requires much effort and high cost that is not good for mass-production. Furthermore, the need of tedious and expensive post-fabrication tuning

and assembling becomes a real problem for manufacturers. Substrate integrated waveguide resonant cavity was proposed at the historic moment. Pilote, Flanik and Zaki were probably the first researchers who developed the idea of replacing the waveguide walls with a series of metallic via holes through the substrate to achieve the same effect of metallic walls [1], [5]. In recent years, pioneering research work on the application and development of SIW techniques have been made in our research center [2], [28]-[34], and both on-substrate metallized via-hole arrays and metallized grooves techniques have been proposed for synthesized waveguide, as shown in Figure 1-1. Therefore, waveguide-based elements and also the entire system can be built on the same substrate that involves active circuits. In addition, the SIW technique can find many applications in which the requirement of weight and volume reduction is essential. In this project, an SIW cavity band-pass filter with pseudo elliptic response has been developed by using the metallized grooves (or slots) technique.

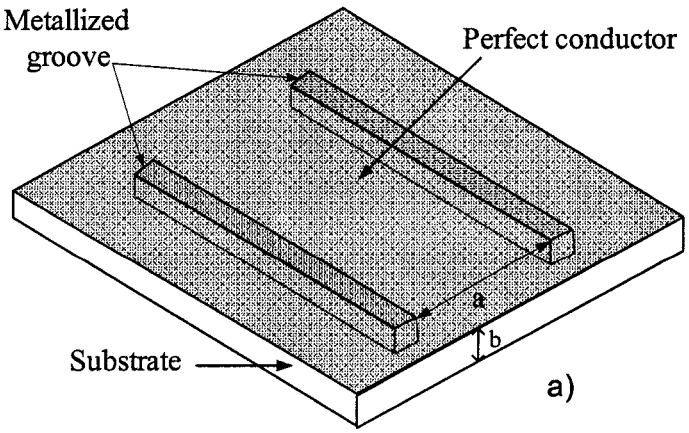

Figure 1-1: On-substrate synthesized waveguide techniques: a) metallized grooves.

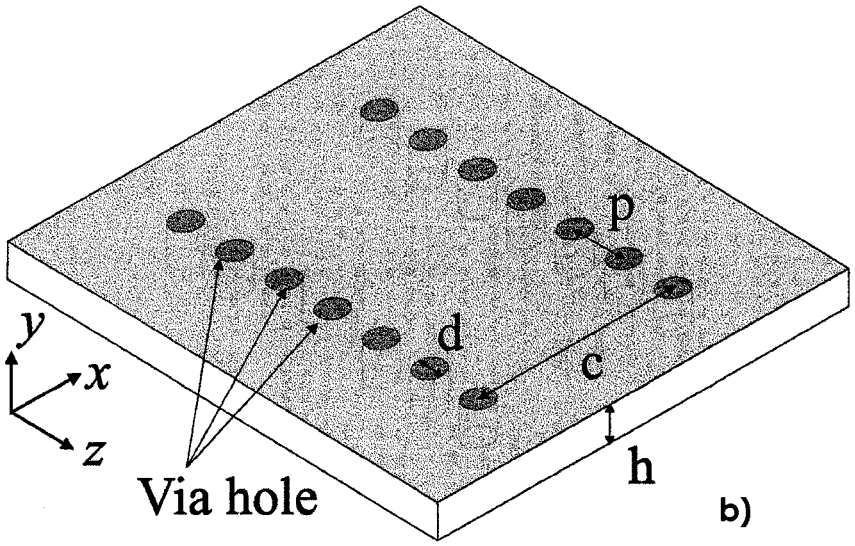

Figure 1- 1: On-substrate synthesized waveguide techniques: b) metallized via-hole arrays (continued).

SIW works like a rectangular waveguide filled with dissipated dielectric material. Typically, there are two types of propagating modes in waveguide called TE and TM modes.

TM mode (Transverse-Magnetic): The magnetic field for this mode is transverse to the direction of propagation, therefore $H_z = 0$. It is also called E mode.

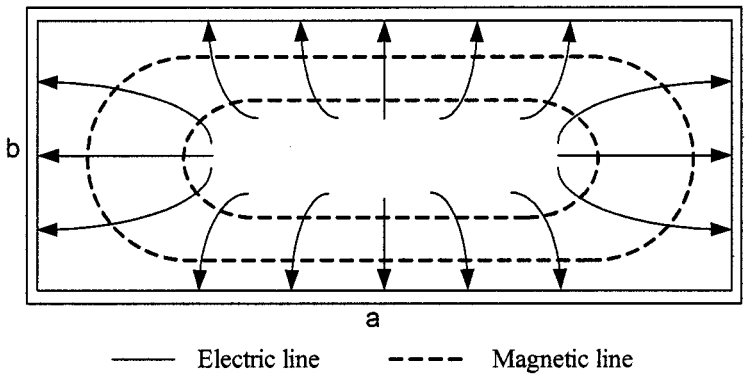

Figure 1- 2: The cross-sectional field distribution in waveguide for TM_{11} mode.

TE mode (Transverse-Electric): The electric field of this mode is transverse to the direction of propagation, therefore $E_z = 0$. It is also called H mode.

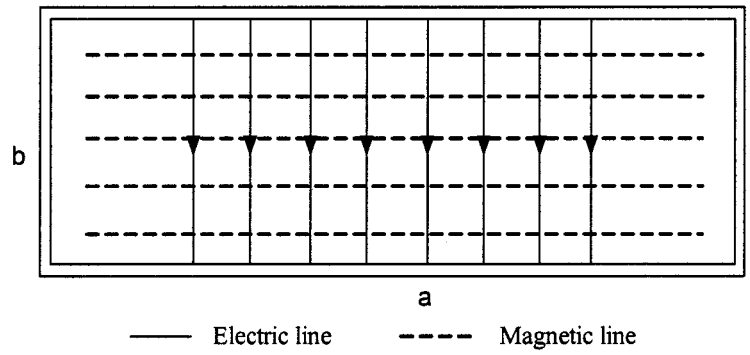

Figure 1- 3: The cross-sectional field distribution in waveguide for TE_{10} mode.

For the substrate integrated waveguide, the TM mode can not be guided because the extremely thin thickness of the substrate. Therefore, the TE mode becomes the sole propagating mode.

1.3. Establishment of coupling scheme

Due to its very thin thickness, the SIW structure points to a fabrication technique that allows the design of a direct coupled planar (H-plane waveguide) cavity filter structure, a coupling method based on the combination of magnetic iris coupling and the transformation of the planar TE_{10n}/TE_{n01} overmoded cavities that were proposed by Uwe Rosenberg [3] is therefore preferred in our SIW filter design.

The principal use of the transformation properties of a TE_{10n}/TE_{n01} mode cavity can be explained by a planar four-poles filter configuration, depicted in figure 1-4, comprising one TE_{102} and three TE_{101} cavities, and there are five main couplings (M_{i1}, M_{12}, M_{23}, M_{34}, M_{4o}) with one non-adjacent coupling M_{14}. The coupling condition of a four-poles elliptic function response with two transmission zeros (TZs) can be expressed by [3]:

$$(M_{12}\ M_{34}) / (M_{23}\ M_{14}) < 0 \qquad (1.3.1)$$

As depicted in figure 1-4 a), three main couplings have the same sign and the remaining non-adjacent coupling shows an opposite one. That is to say, due to the use of the right M_{23} iris location, cavities R1 and R4 exhibit the same magnetic field direction.

A four-pole linear phase filter characteristic results if

$$(M_{12}\ M_{34}) / (M_{23}\ M_{14}) > 0 \qquad (1.3.2)$$

This is depicted in figure 1-4 b), where the left M_{23} iris location is used, which yields a negative cross coupling M_{14}. Consequently, all couplings are negative.

Those physical considerations can be extended to higher-order filter design where the conveniently arranged overmoded TE_{10n} (TE_{n01}) mode cavities are introduced for the transformation properties of 0 and 180 degree phase of the cross couplings for realizing arbitrary filter characteristics.

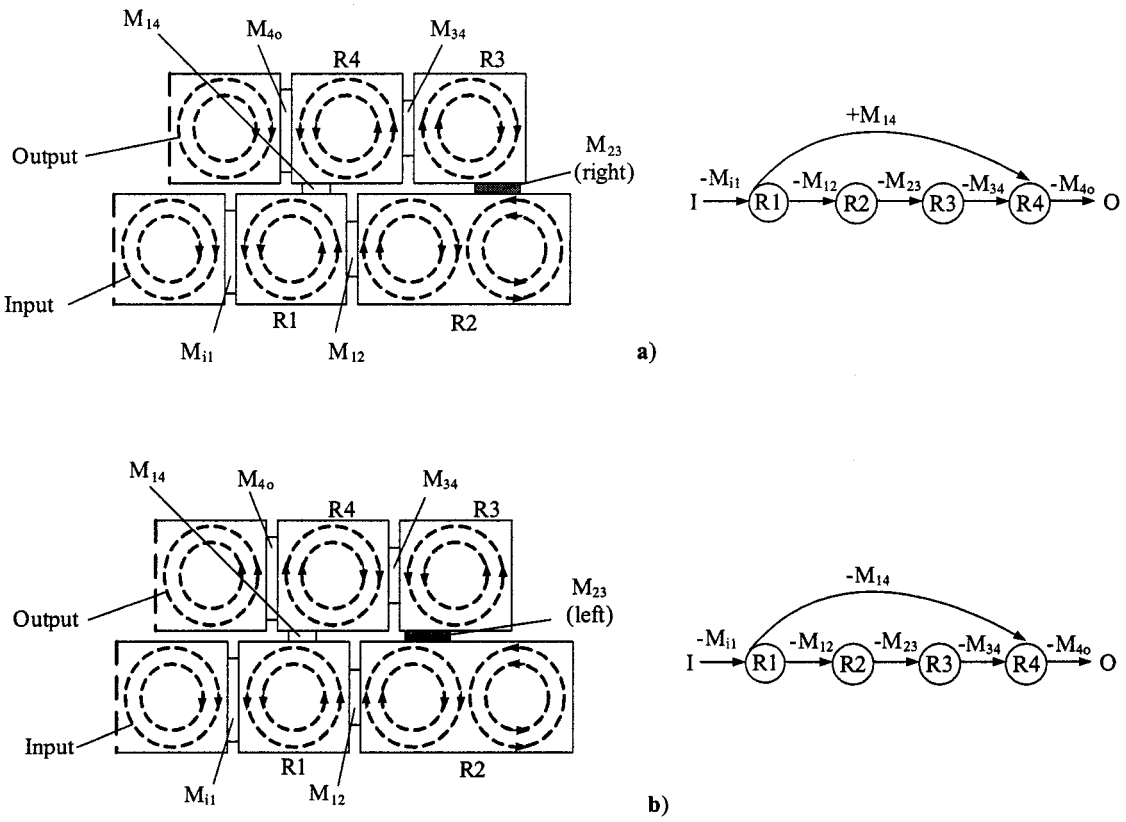

Figure 1- 4: Planar four-pole cavity configuration with three TE101 and one TE102 mode cavities providing cross coupling of first and fourth resonant circuits.
a) Principle magnetic field patterns and coupling schematic for elliptic function response.
b) Principle magnetic field patterns and coupling schematic for linear phase response.

Source: [3]

1.4. Determination of filter specifications and degrees

The pseudo elliptic response filter is preferred in this project to operate at center frequency of 24GHz, with a bandwidth of 3%, i.e., 720MHz, and the in-band return loss should be less than -22dB. From figure 1-4, it can be observed that, in order to generate a positive non-adjacent coupling on the basis of transformation properties of the planar TE_{10n}/TE_{n01} cavities to acquire two TZs, it must make a cavity displacement for cross couplings, which restrict the size of non-adjacent cross coupling iris to be very small, then the non-adjacent coupling could not be strong. It suggests that the two TZs have to be put a little bit far away from the center frequency, which adds difficulties in acquiring symmetric response; this will be explained in detail in Chapter 2. We suppose that two TZs at 22.7GHz and 25.3GHz would be accomplished symmetrically on each side of the passband, then a less than -70dB stop-band insertion loss is expected according to the curves of attenuation versus sharpness given in [6]. Table 1-1 gives the filter specifications.

Center Frequency	**Bandwidth**	**Minimum In-band Return Loss**	**Minimum Out-band Insertion Loss**	**Lower-side TZ**	**Upper-side TZ**
f_0 (GHz)	BW (MHz)	A_{emin} (dB)	A_{min} (dB)	f_{z1} (GHz)	f_{z2} (GHz)
24	720	≥22	≥70	22.7	25.3

Table 1- 1: Filter specifications.

A typical equal-ripple elliptic low-pass prototype characteristic is shown in figure 1-5, Ω_c is the passband cutoff frequency, Ω_s is the equal-ripple stopband start frequency, A_{min} represents the minimum insertion loss in the rejection band. A frequency transformation from the low-pass to band-pass filter has widely been used by the following formula [4]:

$$\Omega = \frac{\omega_0}{\Delta\omega}\left(\frac{\omega}{\omega_0} - \frac{\omega_0}{\omega}\right) \tag{1.4.1}$$

where ω_0 is the center frequency, $\Delta\omega$ is the bandwidth.

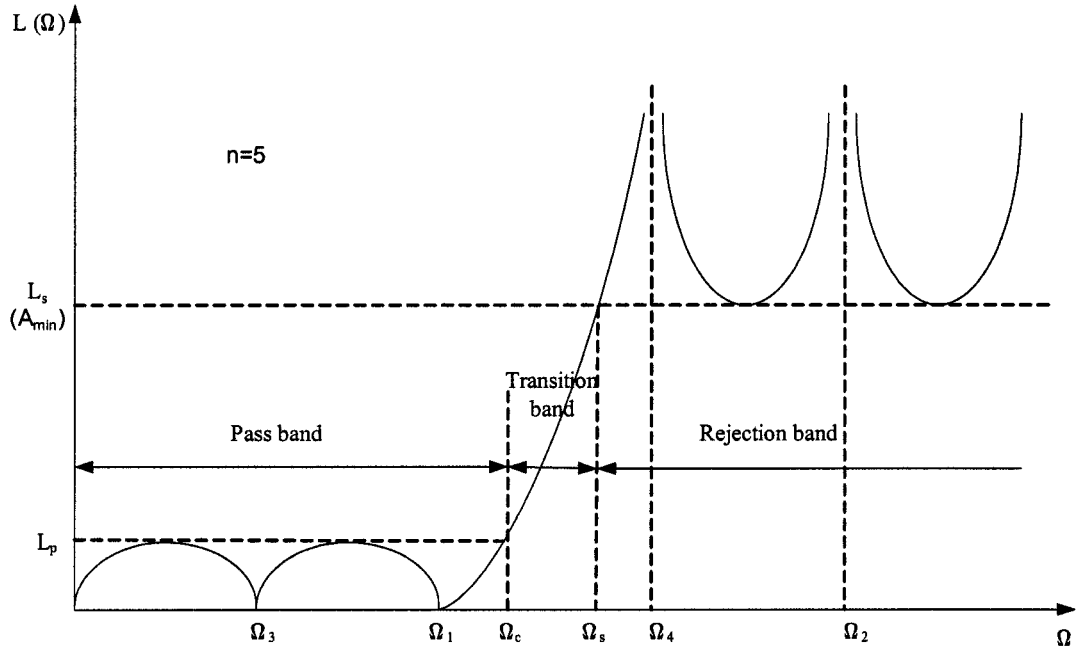

Figure 1- 5: 5-order elliptic low-pass filter prototype.

Based on the filter requirement, some of the above-mentioned band-pass filter parameters can be derivate as the following: f_{-c} = 23.56GHz, f_c = 24.44GHz, f_{-s} = 22.75GHz, f_s = 25.25GHz. Then the order of this band-pass filter can be evaluated by the following procedures [4]:

$$\begin{aligned}
\eta_{-c} &= \sqrt{\frac{f_{-c}}{f_c}} = 0.9818 \\
\eta_c &= \sqrt{\frac{f_c}{f_{-c}}} = 1.0185 \\
\eta_{-s} &= \frac{f_0}{f_s} = 0.9505 \\
\eta_s &= \frac{f_s}{f_0} = 1.0521 \\
\Omega_s &= \frac{\eta_s - \eta_{-s}}{\eta_c - \eta_{-c}} = 2.7684
\end{aligned} \tag{1.4.2}$$

Looking into the curves of attenuation versus sharpness given in [6] and implementing a pseudo elliptic function response band-pass filter with Ω_s=2.7684, $A_{min}+A_{emin} \geq 90$dB, we should use a degree of n=5 to satisfy the specifications.

1.5. Filter synthesis using an analytical gradient-based optimization technique

Frequency invariable coupling matrix has been widely used in the narrow-band cross-coupled resonator band-pass filter synthesis. A number of researchers have given

many kinds of methods on coupling matrix synthesis, e.g., extracting pole, similarity transformations and a series of optimization techniques are presented in [7]-[19]. Among all the existing methods, an analytical gradient-based optimization technique proposed by Smain [19] is much preferred in this project because of its advantages of high efficiency and programmability. This method will be explained in detail in the following steps.

1.5.1. Computation of low-pass prototype filtering function

The class of filtering function that is used here is the generalized Chebyshev function, which is related to the transmission coefficient $S_{21}(\Omega)$ by

$$|S_{21}(\Omega)|^2 = \frac{1}{1+\varepsilon^2 F_N^2(\Omega)} \tag{1.5.1}$$

The ripple level ϵ is related to the minimum in-band return loss R by $\varepsilon = \left[10^{R/10}-1\right]^{-1/2}$. The low-pass prototype frequency Ω has been derived in formula (1.4.1). The filtering function of order N is defined by

$$F_N(\Omega) = \cosh\left[\sum_{n=1}^{N} \cosh^{-1}(x_n)\right] \tag{1.5.2}$$

where x_n is related to the nth transmission zero Ω_n by $x_n = \left(\Omega - 1/\Omega_n\right)/\left(1-\Omega/\Omega_n\right)$.

It can be shown that the function $F_N(\Omega)$ is a rational function whose denominator is given by the product $\prod_{n=1}^{N}(1-(\Omega/\Omega_n))$. The function can therefore be written as

$$F_N(\Omega) = \frac{P_N(\Omega)}{\prod_{n=1}^{N}(1-\frac{\Omega}{\Omega_n})} = \frac{P_N(\Omega)}{D_N(\Omega)} \tag{1.5.3}$$

The numerator $P_N(\Omega)$ is deduced in [19], the following recursion relation is presented:

$$\begin{aligned} P_{N+1}(\Omega) &= -P_{N-1}(\Omega)(1-\frac{\Omega}{\Omega_N})^2 \frac{(1-1/\Omega_{N+1}^2)^{1/2}}{(1-1/\Omega_N^2)^{1/2}} \\ &+P_N(\Omega)[\Omega-\frac{1}{\Omega_{N+1}}+(\Omega-\frac{1}{\Omega_N})\frac{(1-1/\Omega_{N+1}^2)^{1/2}}{(1-1/\Omega_N^2)^{1/2}}] \end{aligned} \tag{1.5.4}$$

The polynomials $P_0(\Omega)$ and $P_1(\Omega)$ are given by

$$P_0(\Omega) = 1, \quad P_1(\Omega) = \Omega - \frac{1}{\Omega_1} \tag{1.5.5}$$

1.5.2. Basic model and its governing equations

A network consisting of N-coupled lossless resonators is shown in Figure 1-6. The frequency independent coupling coefficient between resonators i and j is denoted by $M_{ij}=M_{ji}$. A simple analysis of the network shows that the loop currents, which are grouped in a vector [I], are governed by the following matrix equation [19]:

$$[-jR+\Omega U+M][I]=[A][I]=-j[e] \tag{1.5.6}$$

Here, [U] is the identity matrix, R is a matrix whose only nonzero entries are $R_{11}=R_1$ and $R_{NN}=R_2$, and M is a symmetric square coupling. The excitation vector [e] is given by $[e]^t= [1, 0, 0, \cdots, 0]$ where t is the transposition operator.

Then the scattering parameters can be given by

$$S_{21} = 2\sqrt{R_1 R_2} I_N = -2j\sqrt{R_1 R_2}[A^{-1}]_{N1} \tag{1.5.7}$$

$$S_{11} = 1 - 2R_1 I_1 = 1 + 2jR_1[A^{-1}]_{11} \tag{1.5.8}$$

The synthesis problem can then be formulated by determining the coupling matrix [M] and the resistors R_1 and R_2 such that a prescribed response is reproduced.

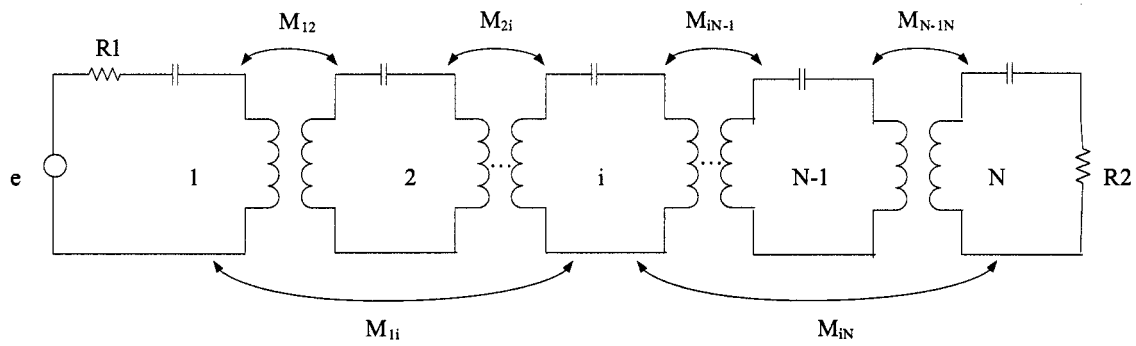

Figure 1- 6: Model of a general cross-coupled resonator bandpass filter.

1.5.3. Error function and gradient calculation

Keeping in mind that the filtering function is the generalized Chebychev prototype which has a rational function of frequency, and that it is uniquely specified by the location of its poles and zeros and an additional scaling constant. Since the zeros of the filtering function are identical to those of S_{11} and its poles are coincident with the zeros of S_{21}, the approach determines the coupling matrix by minimizing a suitable cost function K where the optimization variables are the nonzero entries of the coupling matrix [M] can therefore

be dealt with, K is given by [19]

$$K = \sum_{i=1}^{n} \left| S_{11}(\Omega_{zi}) \right|^2 + \sum_{i=1}^{p} \left| S_{21}(\Omega_{pi}) \right|^2 + \left(\left| S_{11}(\Omega = -1) \right| - \frac{\varepsilon}{\sqrt{1+\varepsilon^2}} \right)^2 + \left(\left| S_{11}(\Omega = 1) \right| - \frac{\varepsilon}{\sqrt{1+\varepsilon^2}} \right)^2 \tag{1.5.9}$$

To make the optimization process more efficient, both the values of the error function and its gradient are used.

$$\begin{aligned}
&\frac{\partial S_{11}}{\partial M_{pq}} = -4jR_1 P_{pq} [A^{-1}]_{1p} [A^{-1}]_{q1} \\
&\frac{\partial S_{21}}{\partial M_{pq}} = 2j\sqrt{R_1 R_2} P_{pq} ([A^{-1}]_{Np} [A^{-1}]_{q1} + [A^{-1}]_{Nq} [A^{-1}]_{p1}) \\
&\frac{\partial S_{11}}{\partial M_{pp}} = -2jR_1 P_{pp} [A^{-1}]_{p1} [A^{-1}]_{p1} \\
&\frac{\partial S_{21}}{\partial M_{pp}} = 2j\sqrt{R_1 R_2} P_{pp} [A^{-1}]_{Np} [A^{-1}]_{p1} \\
&\frac{\partial S_{11}}{\partial R_1} = 2j[A^{-1}]_{11} + 2R_1 ([A^{-1}]_{11} [A^{-1}]_{11} + r[A^{-1}]_{N1} [A^{-1}]_{N1}) \\
&\frac{\partial S_{21}}{\partial R_1} = -2j\sqrt{r}[A^{-1}]_{N1} + 2R_1\sqrt{r}([A^{-1}]_{N1} [A^{-1}]_{11} + r[A^{-1}]_{NN} [A^{-1}]_{N1}
\end{aligned} \tag{1.5.10}$$

where the ratio of the two resistors is specified as R_2=r R_1.

Conforming to the previous descriptions, stating that in order to accomplish the desired filter specifications, a degree of n=5, with one non-adjacent cross-coupling structure must to be established. Also relying on the adopted coupling scheme, a filter topology is proposed in Figure 1-7. Thus, a coupling matrix M should be developed in the form of

$$M = \begin{bmatrix} M_{11} & M_{12} & 0 & 0 & 0 \\ M_{12} & M_{22} & M_{23} & 0 & M_{25} \\ 0 & M_{23} & M_{33} & M_{34} & 0 \\ 0 & 0 & M_{34} & M_{44} & M_{12} \\ 0 & M_{25} & 0 & M_{12} & M_{55} \end{bmatrix} \quad (1.5.11)$$

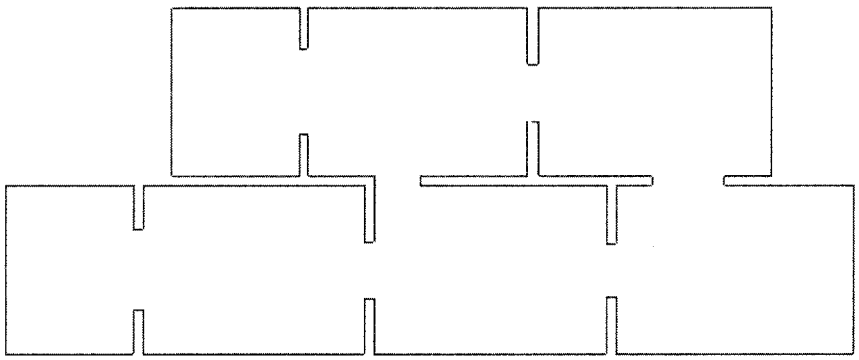

Figure 1- 7: Filter topology

1.5.4. Calculation of group delay

Often the group delay is nothing more than the phase delay, this happens when the phase delay is independent of frequency. In some applications such as multiplexing filters for communication systems, it is important to have a linear phase response in the passband to avoid signal distortion. So the phase response of the filter must be deliberately synthesized, usually resulting in an inferior amplitude cutoff characteristic. For the elliptic function filter, the sharp-cutoff amplitude response is generally incompatible with a good phase response. In this case, it can be shown that the group delay τ_g is given by [19]

$$\tau_g = -\mathrm{Im}\left[\frac{1}{S_{21}}\frac{\partial S_{21}}{\partial \Omega}\right] \tag{1.5.12}$$

Recalling that Ω is a normalized and transformed frequency variable as shown in formula (1.4.1), the actual value of the group delay should take this transformation into consideration.

Following similar steps to those in the previous section and using the fact that the derivative of the matrix [A] with respect to Ω is equal to the identity matrix, the group delay can be obtained by

$$\tau_g = \mathrm{Im}\left[\frac{\sum_{k=1}^{N}\left[A^{-1}\right]_{Nk}\left[A^{-1}\right]_{k1}}{\left[A^{-1}\right]_{N1}}\right] \tag{1.5.13}$$

A MATLAB code which describes the above optimization principle is attached in the Appendix, the coupling matrix with the two resistors R_1 and R_2 in connection with this project can be achieved for $R_1 = R_2 = 1.077$

$$\mathrm{M} = \begin{bmatrix} 0 & 0.925 & 0 & 0 & 0 \\ 0.925 & 0 & 0.658 & 0 & -0.024 \\ 0 & 0.658 & 0 & 0.676 & 0 \\ 0 & 0 & 0.676 & 0 & 0.925 \\ 0 & -0.024 & 0 & 0.925 & 0 \end{bmatrix} \tag{1.5.14}$$

The synthesized scattering parameter response and group delay can be shown in Figure 1-8.

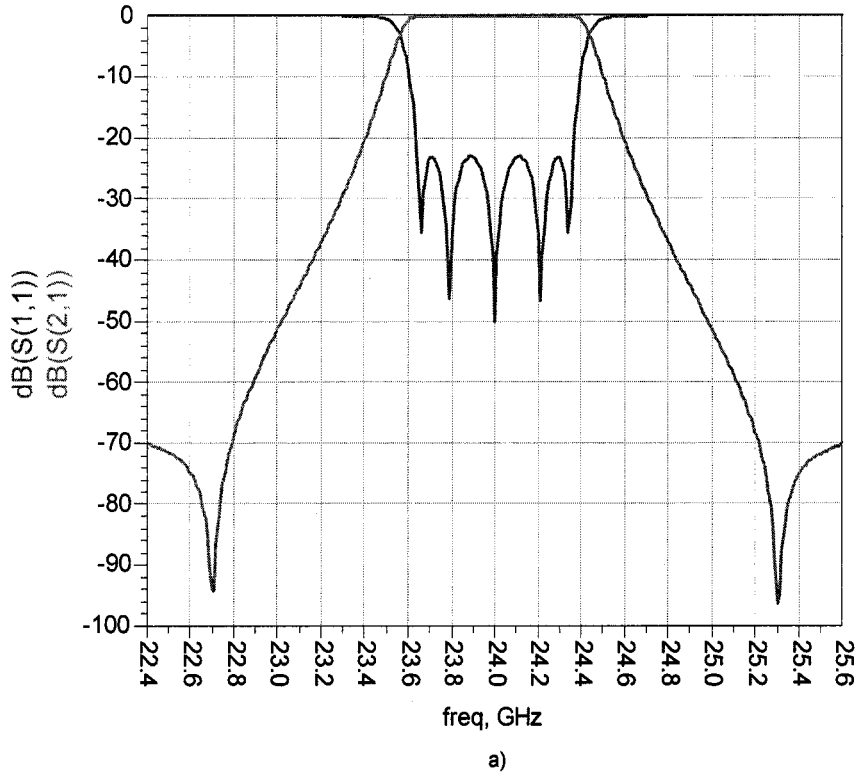

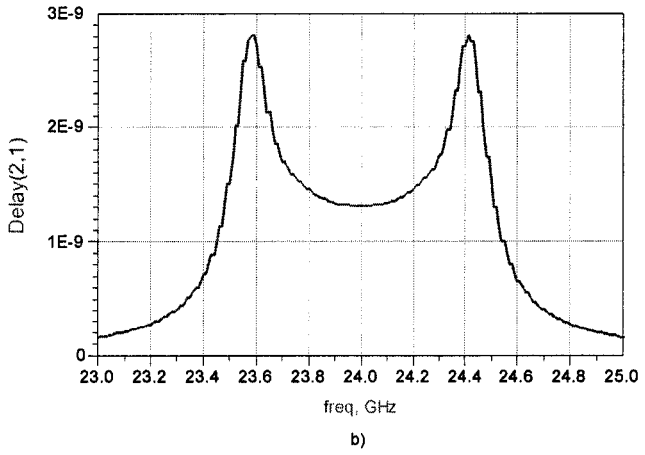

Figure 1- 8: synthesized filter responses: a) insertion and return loss, and b) group delay.

Chapter 2. PHYSICAL REALIZATION OF PSEUDO-ELLIPTIC FILTER

2.1. Introduction

Substrate material will be chosen by considering both the manufacture process and cavity quality factor Q requirements. Based on the coupling matrix, the source and the load resistors can be obtained from the synthesis process, initial dimensions of the SIW resonant cavities and coupling slots can be determined by using a commercial finite element method (FEM) simulator HFSS. A tuning effort will be invested with HFSS to correct the initial dimensions in order to generate the desired response. It will be demonstrated finally that for high-order asymmetric cross-coupling filter structures, the coupling matrix synthesis process based on a mode matching technique or physical dimension optimization process is inevitable for obtaining a post-tuning free design.

2.2. Choose of substrate material

To begin with the resonant cavity design, a substrate material has to be chosen first. Considering the present fabrication available in our research center and the technology

maturity and fabrication precision, a new fabrication process developed in our center will be deployed and a material of ceramic with high hardness and very thin thickness is considered. Some of the material parameters are presented in Table 2-1.

Substrate ® 996	Typical Values
Dielectric Constant @1MHz	9.9
Loss Tangent @1MHz	0.0001
Alumina Content (nominal)	99.6 (Weight%)
Coefficient of Linear Thermal Expansion	Unit (ppm/°C)
25°-300°C	7.0
25°-600°C	7.2
25°-800°C	7.9
25°-1000°C	8.2
Hardness	87
Thickness	0.254 mm
Volume Resistivity	Unit (ohm-cm)
25°C	>1.0E+14
100°C	>1.0E+14
300°C	>1.0E+13
500°C	>1.0E+10
700°C	>1.0E+9

Table 2- 1: Substrate characteristics.

In rectangular waveguide, it has been well known that the propagation constant β of electromagnetic wave can be derived by

$$\beta = \sqrt{K^2 - \left(\frac{m\pi}{a}\right)^2 - \left(\frac{n\pi}{b}\right)^2} \tag{2.2.1}$$

Here, $K = \omega\sqrt{\mu\varepsilon}$, ε and μ are the dielectric permittivity and permeability, m and n represents the half-wave number in x and y direction respectively. For the SIW, its cross-sectional dimensions should be calculated based on the operating frequency and the dominant propagation mode in the same way as what is usually done for the rectangular waveguide. Because the dominant propagation mode used here is TE_{10} mode, it can be seen from formula (2.2.1) that its propagation constant β is only related to the width "a" due to m=1, n=0. Therefore, the height or thickness "b" in y direction, as shown in Figure 2-1, can arbitrarily be chosen without impact on TE_{10} mode propagation, hence allowing its integration into a thin substrate. Reduction of the height "b" could lead to a less radiation loss of the microstrip line, however, it would increase the conductor loss in both the microstrip line and rectangular waveguide. Its impact on the quality factor Q of rectangular resonant cavity will be discussed in the following sections.

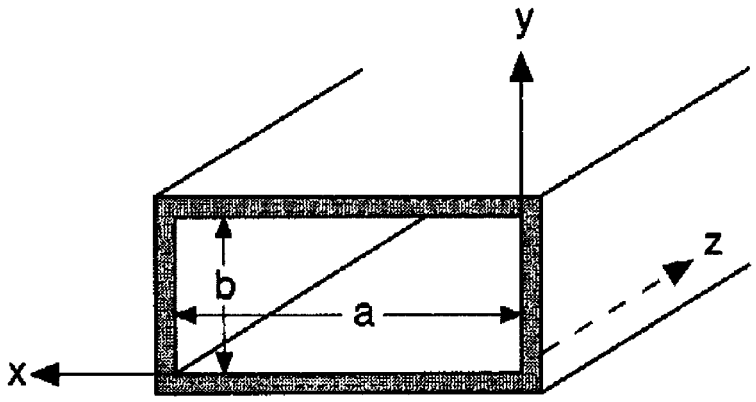

Figure 2- 1: Rectangular waveguide.

2.3. Design of rectangular waveguide cavity

The rectangular resonant cavity is the main element in waveguide filter design. It consists of a rectangular waveguide section with a fixed length of "L" and terminated in short-circuit in both ends, in another words, it is a closed rectangular waveguide box filled with one or more kinds of dielectrics, as is shown in Figure 2-2.

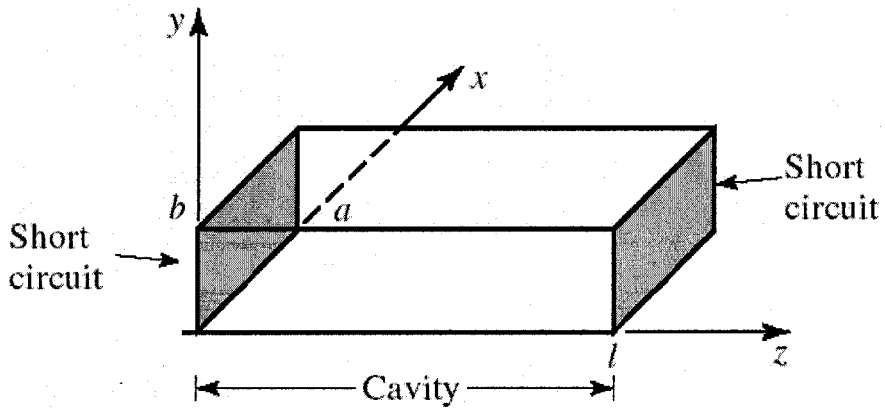

Figure 2- 2: Rectangular waveguide resonant cavity.

In the rectangular waveguide cavity, the E field transverse component (E_x, E_y) of the TE_{mn} or TM_{mn} modes can be expressed as [20]:

$$E_t(x,y,z) = E_{0t}(x,y)\left[A^+ e^{-j\beta_{mn}z} + A^- e^{j\beta_{mn}z}\right] \tag{2.3.1}$$

Here, E_{0t} (x, y) is the transverse coordinate function of the transverse E field; A^+ and A^- are arbitrary amplitude coefficients of the forward and reverse traveling waves. As has already been discussed in the above section, the propagation constant of the TE_{mn} mode can be expressed as:

$$\beta = \sqrt{K^2 - \left(\frac{m\pi}{a}\right)^2 - \left(\frac{n\pi}{b}\right)^2} \tag{2.3.2}$$

Substituting the boundary condition $E_t = 0$ at z=0 into the above formula, $A^- = -A^+$ can be obtained. Again, from the boundary condition $E_t = 0$ at z=L, it yields:

$$E_t(x,y,l) = -E_{0t}(x,y)A^+ 2j\sin\beta_{mn}l = 0 \tag{2.3.3}$$

Consequently,

$$\beta_{mn} = \frac{p\pi}{l} \qquad \text{p=1, 2, } \cdots \tag{2.3.4}$$

This means, the length of the resonant cavity must be integer times of the half waveguide wavelength at resonant frequency.

The cutoff wave number of the rectangular cavity also can be given by:

$$k_{c_{mnp}} = \sqrt{\left(\frac{m\pi}{a}\right)^2 + \left(\frac{n\pi}{b}\right)^2 + \left(\frac{p\pi}{l}\right)^2} \tag{2.3.5}$$

the subscripts m, n and p represent the half stationary wave numbers which are related

to the dimensions of a, b and *l*, respectively. The resonant frequency of the TE_{mn} modes is thus derived as:

$$f_{mnp} = \frac{ck_{mnp}}{2\pi\sqrt{\mu_r\varepsilon_r}} = \frac{c}{2\pi\sqrt{\mu_r\varepsilon_r}}\sqrt{\left(\frac{m\pi}{a}\right)^2 + \left(\frac{n\pi}{b}\right)^2 + \left(\frac{p\pi}{l}\right)^2} \tag{2.3.6}$$

As is shown in Table 2-1, the SIW thickness or height "b" has been fixed at 10 mil, the subsequent procedure is to determine width "a" and length "*l*" of the SIW rectangular resonant cavity. To the rectangular waveguide, the premier requirement for choosing the cross-sectional dimensions is to guarantee that only the dominant propagation mode TE_{10} mode will be guided. Figure 2-3 gives us a distinct modal distribution from which it can be seen that the principle of choosing the waveguide cross-sectional dimensions could be made by

$$\left.\begin{matrix}\lambda_{cTE_{20}} \\ \lambda_{cTE_{01}}\end{matrix}\right\} \prec \lambda \prec \lambda_{cTE_{10}} \tag{2.3.7}$$

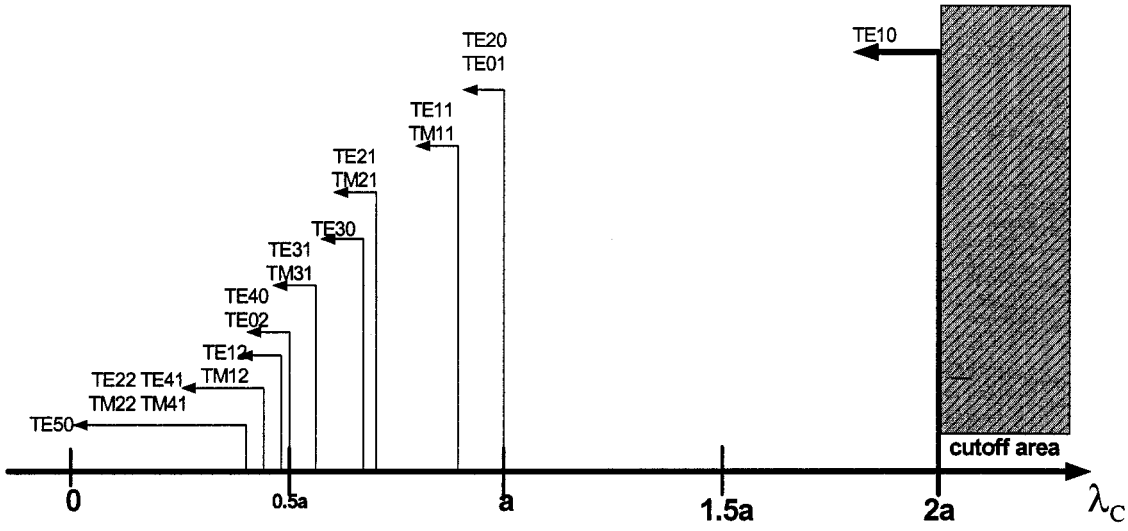

Figure 2- 3: Distribution graphic of cutoff wavelengths in rectangular waveguide.

The cutoff wavelength of the TE_{mn} modes of the air-filled rectangular waveguide is given by:

$$\lambda_{c_{mn}} = \frac{2\pi}{k_{c_{mn}}} = \frac{2}{\sqrt{\left(\frac{m}{a}\right)^2 + \left(\frac{n}{b}\right)^2}} \tag{2.3.8}$$

Hence, the formula (2.3.7) is equal to:

$$\left.\begin{matrix} a \\ 2b \end{matrix}\right\} \prec \lambda \prec 2a \tag{2.3.9}$$

That is to say,

$$\begin{aligned} \lambda/2 &\prec a \prec \lambda \\ 0 &\prec b \prec \lambda/2 \end{aligned} \tag{2.3.10}$$

For 24GHz, the wavelength is $\lambda = c/f = 492.1mil$, referring to the dimension of standard air-filled waveguide WR-42, which has the "a" being 420mil. Therefore for the

SIW with a relative permittivity of $\varepsilon_r = 9.9$ (see Table 2-1), the parameters should be modified as $a = 420/\sqrt{\varepsilon_r} = 133.5mil$, $\lambda = 492.1/\sqrt{\varepsilon_r} = 156.4mil$. As has been demonstrated in Chapter 1, the TE_{102} mode will be used as the dominant resonant mode. From formula (2.3.8), it can be observed that, for TE_{10} mode, its cutoff wavelength is $\lambda_c = 2a = 267mil$. Then, its waveguide wavelength should be calculated as:

$$\lambda_g = \frac{\lambda}{\sqrt{1-\left(\frac{\lambda}{\lambda_c}\right)^2}} = 193mil \tag{2.3.11}$$

For TE_{102} resonant mode, the rectangular resonant cavity length "*l*" should be equivalent to two stationary wave numbers, i.e., $l = \lambda_g$.

In conclusion, the SIW rectangular resonant cavity is designed by selecting width a=133.5mil, height b=10mil, length *l*=193mil.

2.4. Analysis of Q factor and loss

The quality factor Q is a specification parameter which points to the frequency selectivity of the microwave resonant system and also the relationship between the energy storage and the loss in the resonator. It can be defined as:

$$Q = 2\pi \frac{\text{maximum energy stored per cycle}}{\text{Energy dissipated per cycle}} \tag{2.4.1}$$

For rectangular waveguide cavity resonator, its unloaded quality factor Q can also be expressed as:

$$Q_u = \left(\frac{1}{Q_c} + \frac{1}{Q_d} \right)^{-1} \tag{2.4.2}$$

Here, Q_c is the quality factor of the TE_{10n} mode rectangular cavity with finite conductor wall but lossless dielectric [20].

$$Q_c = \frac{(kal)^3 b\eta}{2\pi^2 R_s} \frac{1}{\left(2n^2a^3b + 2bl^3 + n^2a^3l + al^3\right)} \tag{2.4.3}$$

where k is the wave number defined by $k = \omega\sqrt{\mu\varepsilon}$. The intrinsic impedance is calculated by $\eta = \frac{377}{\sqrt{\varepsilon_r}}$. Rs is the surface resistivity which could be calculated from $R_s = \sqrt{\frac{\omega\mu_0}{2\sigma}}$, σ is the metal conductivity, μ_0 is vacuum permeability.

Q_d is the Q value of the rectangular resonator with perfect conductor wall but dissipated dielectric:

$$Q_d = \frac{1}{tg\delta} \tag{2.4.4}$$

where $tg\delta$ is the dielectric dissipation factor.

For this SIW cavity filter, as has been analyzed in the above paragraphs, the well-defined parameters are: $f_0 = 24GHz$, $\varepsilon_r = 9.9$, a=133.5mil, $b = 10mil$,

$l = 193mil$, $\mu_0 = 4\pi \times 10^{-7} H/m$, $\sigma = 5.8 \times 10^7 s/m$ (copper), $tg\delta = 0.0001$. On the basis of the above formulas, Q_u can thus be obtained and its value is $Q_u = 522$. This can also be verified by using a commercial package (ANSOFT) with $Q_u = 517$. It is observed that these two Q_u are almost the same. Another expression for Q_u is [20]:

$$Q_u \approx \frac{1}{\delta} \frac{V}{S} \tag{2.4.5}$$

It means Q_u is approximately in direct proportion to the cavity volume V, in inverse proportion to the cavity inside surface area S and the skin depth δ. Therefore, in order to achieve a high Q value, a higher value of V/S should be considered. For this filter design, increasing Q needs to increase the substrate thickness "b", which increases the complexity and tolerance during the fabrication process; it needs effort to carry out more investigations. Another way for Q improvement is to use silver instead of copper to increase Q_c then Q_u.

The overall in-band insertion loss (IL) of the band-pass filter can roughly be evaluated by [21]:

$$L_A = \frac{4.343n}{wQ_u} \tag{2.4.6}$$

where n is the filter order, w is the fractional bandwidth. So, an evaluated value of $IL = 1.4dB$ can be obtained for our filter. This is only a very rough prediction of the in-band insertion loss. In reality, extra loss will also be caused by the input and output

transitions with the microstrip line and by radiation. Thus, a higher value of IL is expected in practical applications.

During the synthesis process of the desired transmission coefficients response, dissipation effects can be accounted for by simply replacing the frequency variable $j\Omega$ for the lossless circuit by $(j\Omega + d)$ to include the losses in which $d = 1/wQ_u$ [21]. Reevaluating the scattering parameters S_{11} and S_{21} responses by this substitution using the synthesis method described in Chapter 1, we can obtain the following response curves in Figure 2-4:

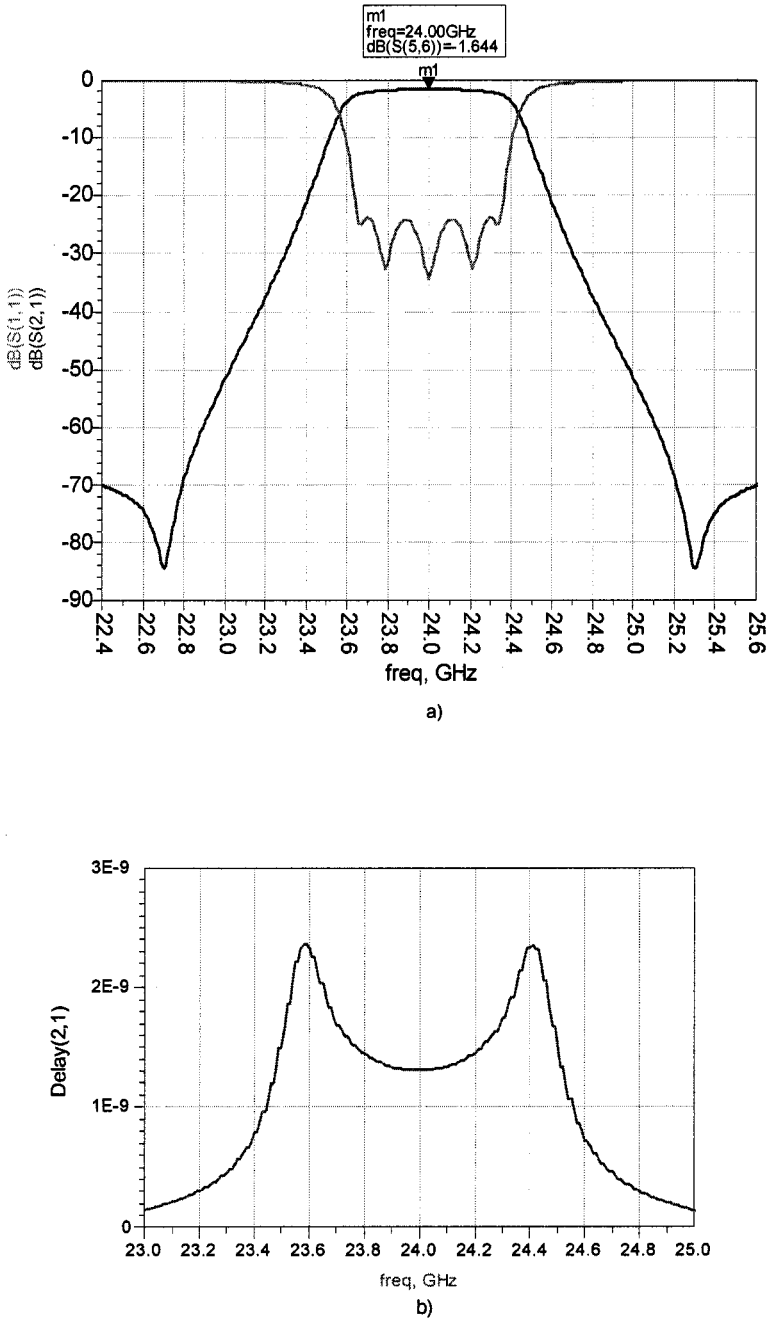

Figure 2- 4: Synthesized filter responses considering the loss effects: a) insertion and return loss and b) group delay.

It shows that due to a lower Q value, a higher in-band insertion loss of around 1.64dB is encountered that confirms the above analysis, and the TZs rejection can not be made as sharp as has been shown in Figure 1-8. However, the overall performance as shown in Table 1-1 can be fulfilled without problem; this means the quality factor Q can satisfy the requirements for implementing our pseudo-elliptic function filter. Then, the design could be carried out into the physical realization stage.

2.5. Calculation of the initial dimensions

2.5.1. Conception of impedance inverter K

Figure 2-5 shows a lumped elements-based band-pass filter two-port network. Since an arrangement consisting of alternate series and parallel resonators is difficult to implement in microwave circuits, it is a quite practical approach to replace the parallel-resonant circuits of the band-pass filter by impedance inverters or impedance inverting transformers as shown in figure 2-6.

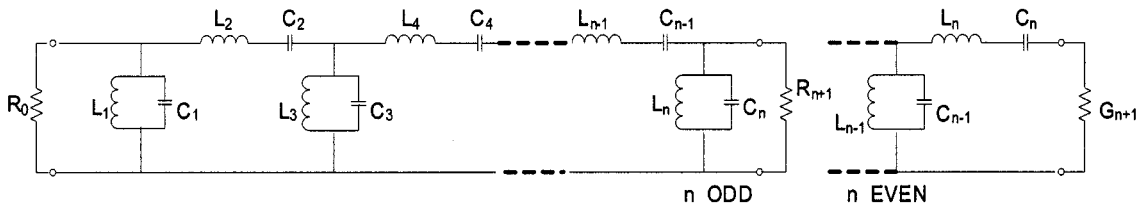

Figure 2- 5: Lumped elements band-pass filter.

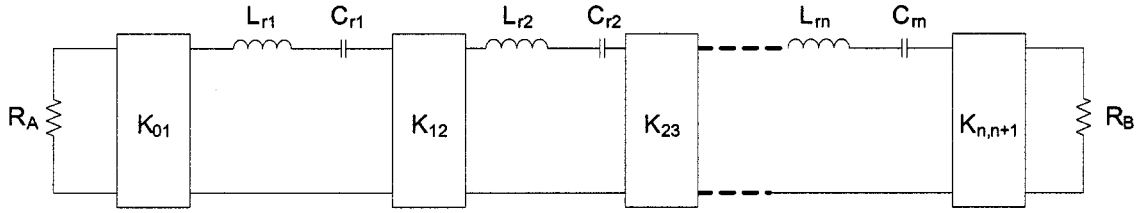

Figure 2- 6: Band-pass filter containing impedance inverters.

An impedance inverter is a lossless, reciprocal, frequency-independent, two-port network, defined by its ABCD matrix [22]

$$\begin{bmatrix} A & B \\ C & D \end{bmatrix} = \begin{bmatrix} 0 & jK \\ j/K & 0 \end{bmatrix} \tag{2.5.1}$$

From the ABCD matrix, its scattering parameters can be deduced

$$\begin{aligned} |S_{11}| = |S_{22}| &= \left| \frac{(K/Z_0)^2 - 1}{(K/Z_0)^2 + 1} \right| \qquad \angle S_{11} = \angle S_{22} = \pm 180° \\ |S_{21}| = |S_{12}| &= \left| \frac{2K/Z_0}{(K/Z_0)^2 + 1} \right| \qquad \angle S_{21} = \angle S_{12} = \pm 90° \end{aligned} \tag{2.5.2}$$

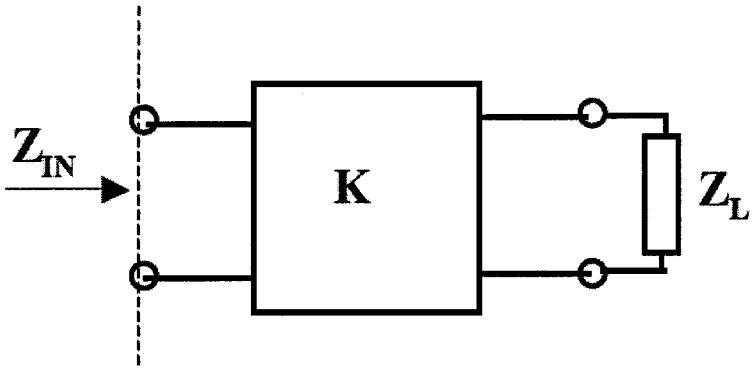

Figure 2- 7: Impedance inverter terminated in a load.

The main property of an inverter is that of impedance inversion. Considering the circuit of Figure 2-7 that consists of an impedance inverter which is terminated in a load Z_L. According to the definition of K,

$$Z_{IN} = \frac{AZ_L + B}{CZ_L + D} = \frac{jK}{jZ_L/K} = \frac{K^2}{Z_L} \tag{2.5.3}$$

There are many kinds of methods to realize the impedance inverter, one typical impedance inverter circuit is shown in Figure 2-8, where Φ is the electrical length of impedance inverter (usually negative numbers) [21].

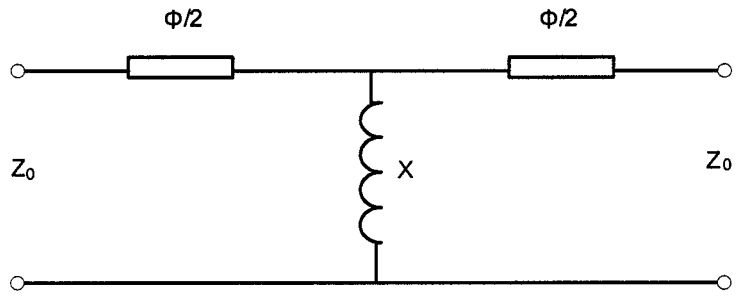

Figure 2- 8: Typical impedance inverting circuit.

$$K = \left| Z_0 tg(\phi/2) \right|$$
$$\Phi = -tg^{-1}(2X/Z_0) \qquad (2.5.4)$$
$$X/Z_0 = \frac{K/Z_0}{1-(K/Z_0)^2}$$

The negative electrical length of the impedance inverter can be incorporated into the length of individual resonator, the electric length of resonator (half wave) will then be reduced to

$$\theta_j = \pi + \frac{1}{2}\left[\phi_{j-1,j} + \phi_{j,j+1}\right] \quad j \in (1,n) \qquad (2.5.5)$$

Therefore, physical lengths of the resonators are obtained by simply multiplying the electrical length by the guided wavelength divided by 2π .

In our case, the coupling slots among waveguide resonant cavities act as impedance inverters. If the scattering parameters of all the coupling slots are available from the transformation of the desired coupling coefficients which have already been synthesized in Chapter 1, the initial dimensions of the coupling slots will be achieved by doing simulation with the commercial package HFSS, and the length of cavities will be modified by using formula (2.5.4).

2.5.2. Transformation of coupling coefficients M_{ij}

From reference [21], the following transformation procedure can be developed step by step. Starting from the normalized coupling matrix which has already been described in

the filter synthesis section of Chapter 1, where n is the order of the filter.

$$M = \begin{bmatrix} M_{11} & \cdots & M_{1n} \\ \vdots & \ddots & \vdots \\ M_{n1} & \cdots & M_{nn} \end{bmatrix}_{n \times n}$$

The following development is valid only for a symmetrical filter ($M_{ii} = 0$) with one coupling for the source and the load ($M_{Si} = 0$ if $i \neq 1$ and $M_{jL} = 0$ if $j \neq n$).

The coupling coefficient between the first cavity and the source, and the one between the N^{th} cavity and the load can be calculated as (R_s and R_l are source and load resistances respectively):

$$M_{S1} = M_{1S} = \pm\sqrt{R_s}, \quad M_{nL} = M_{Ln} = \pm\sqrt{R_l} \tag{2.5.6}$$

The sign for the coupling must be the same as the sign for the direct coupling in the filter (direct path). Then, the following developed coupling matrix will be obtained:

$$M = \begin{bmatrix} 0 & M_{S1} & \cdots & 0 & 0 \\ M_{1S} & M_{11} & \cdots & M_{1n} & 0 \\ \vdots & \vdots & \ddots & \vdots & \vdots \\ 0 & M_{n1} & \cdots & M_{nn} & M_{nL} \\ 0 & 0 & \cdots & M_{Ln} & 0 \end{bmatrix}_{n+2 \times n+2}$$

From the above normalized coupling matrix M the de-normalized coupling coefficient k will be calculated from these equations:

$$\begin{aligned} k_{S1} &= M_{S1} \times \sqrt{Bw / f_0} \\ k_{ij} &= M_{ij} \times Bw / f_0 \\ k_{nL} &= M_{nL} \times \sqrt{Bw / f_0} \end{aligned} \tag{2.5.7}$$

Bw is the bandwidth and f_0 is the center frequency.

Then, we can compute the normalized impedance inverter K values from the de-normalized coupling coefficient k:

$$\begin{aligned}
\frac{K_{01}}{Z_0} &= k_{S1} \times \sqrt{\frac{l_1 \pi}{2} \frac{\lambda_g}{\lambda_0}} \\
\frac{K_{ij}}{Z_0} &= k_{ij} \times \frac{\pi}{2} \sqrt{l_i l_j} \times \frac{\lambda_g}{\lambda_0} \\
\frac{K_{n,n+1}}{Z_0} &= k_{nL} \times \sqrt{\frac{l_n \pi}{2} \frac{\lambda_g}{\lambda_0}}
\end{aligned} \tag{2.5.8}$$

where l is the number of half-wavelength in the resonator, λ_0 and λ_g are the wavelength and waveguide wavelength at the center frequency, respectively.

Finally, the scattering parameters of each coupling structure can be calculated by applying formula (2.5.2).

Adhering to the above step-by-step procedure based on the desired coupling coefficients matrix (1.5.14), we obtain the desired scattering parameters of each coupling structure as following:

$$
\begin{aligned}
|S_{11}|_{s1} &= |S_{22}|_{s1} = 0.7623, & |S_{21}|_{s1} &= |S_{12}|_{s1} = 0.6472 \\
|S_{11}|_{12} &= |S_{22}|_{12} = 0.9771, & |S_{21}|_{12} &= |S_{12}|_{12} = 0.2128 \\
|S_{11}|_{23} &= |S_{22}|_{23} = 0.9877, & |S_{21}|_{23} &= |S_{12}|_{23} = 0.1563 \\
|S_{11}|_{34} &= |S_{22}|_{34} = 0.9884, & |S_{21}|_{34} &= |S_{12}|_{34} = 0.1522 \\
|S_{11}|_{45} &= |S_{22}|_{45} = 0.9771, & |S_{21}|_{45} &= |S_{12}|_{45} = 0.2128 \\
|S_{11}|_{5l} &= |S_{22}|_{5l} = 0.7623, & |S_{21}|_{5l} &= |S_{12}|_{5l} = 0.6472 \\
|S_{11}|_{25} &= |S_{22}|_{25} = 0.99998, & |S_{21}|_{25} &= |S_{12}|_{25} = 0.00566
\end{aligned}
\tag{2.5.9}
$$

Now, two sections of dielectric waveguide are built with a length of λ_g, and they are coupled by one slot with a fixed thickness of "t" as shown in Figure 2-9. Couplings between input and resonant cavities 1 (R1), R1 and R2, R2 and R3, R4 and R5, R5 and output take place on broadside wall as shown in Figure 2-9a. Couplings between R3 and R4, R2 and R5 are related to side-wall with one broad-side of each cavity to be shorted as shown in Figure 2-9b. With the HFSS simulation at 24GHz, and changing the width of the slots until the simulated $|S_{21}|$ equal the reference values in (2.5.9). Repeating this process one by one, the initial dimensions of slots widths "h" can be obtained, and also the initial dimensions of cavities lengths "l" can be calculated from formula (2.5.5). In conclusion, all the initial dimensions are obtained as follows:

$$
\begin{aligned}
&h_{s1} = h_{5l} = 64.6mil, \quad h_{12} = h_{45} = 46.2mil \\
&h_{23} = 40.1mil, \; h_{34} = 58mil, \; h_{25} = 20.7mil \\
&l_1 = 170mil, \; l_2 = 177.2mil, \; l_3 = 188.4mil \\
&l_4 = 185.1mil, \; l_5 = 169mil, \; t = 12mil
\end{aligned}
\tag{2.5.10}
$$

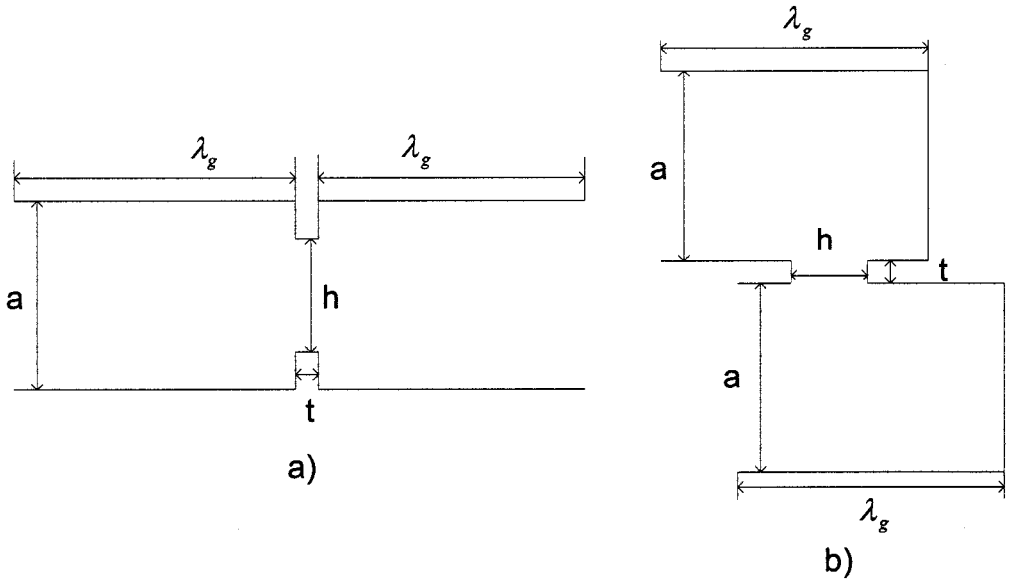

Figure 2- 9: Filter coupling structures: a) Broadside-wall coupling structure for tuning of h_{s1}, h_{12}, h_{23}, h_{45} and h_{5l}; and b) side-wall coupling structure for tuning of h_{34} and h_{25}.

By applying the initial dimensions to the filter topology and carrying out the simulation with HFSS, the following scattering parameter responses are generated:

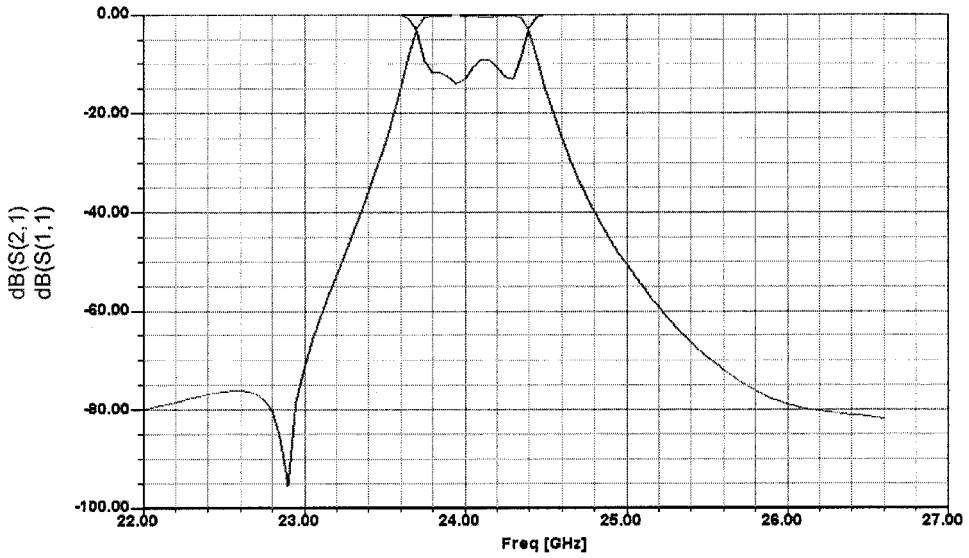

Figure 2- 10: S_{11} and S_{21} responses with the initial dimensions.

2.6. Tuning and optimization

From Figure 2- 10, it can be seen that with the initial dimensions, the in-band return loss is only around -10dB, the right side TZ is not fulfilled significantly, an efficient tuning method must be developed. Jan and Kjetil [23] suggested a tuning procedure which was implemented by using a mode-matching/finite element program Wasp-Net for symmetrical waveguide filters with cross couplings in the E-plane. This innovative method will be studied for our asymmetrical H-plane coupled SIW cavity filter structure with some modification related to our own topology characteristics. In the following, the tuning procedure is described in detail in several steps.

Step 1, simulating cavity 1, 3 and 4 respectively as shown in Figure 2- 11, sweeping

for 20 frequency points. For $|S_{21}|$, this results in a curve with a single peak at the resonant frequency of the cavity. Adjusting the cavity length until the peak is at 24GHz.

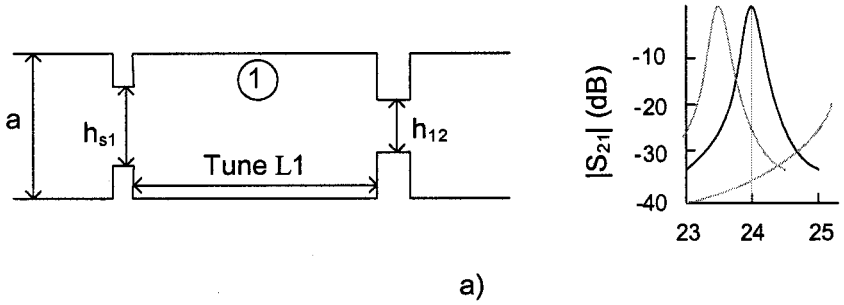

a)

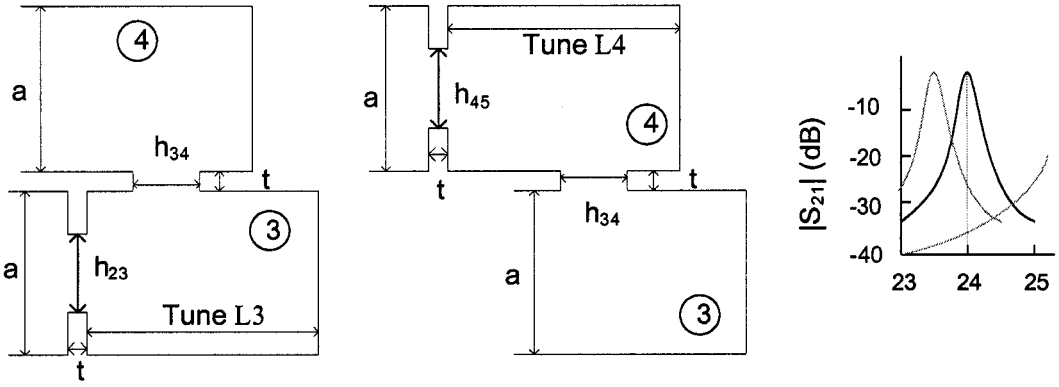

b)

Figure 2- 11: Step 1 for cavity length tuning by sweeping 20 frequency points in HFSS: a) Length tuning of cavity 1 and b) Length tuning of cavity 3 and 4.

Step 2, simulating the structures shown in Figure 2- 12, in which the coupling between cavities 2 and 3 and also the coupling between cavities 4 and 5 of the complete filter are replaced by a shorted wall. Finding a new length for cavities 2 and 5 by adjusting the cavity length until the peak of $|S_{21}|$ is at 24GHz. Then, using the new cavity lengths to tune the cross-coupling slot width h_{25} again until the simulated $|S_{21}|$ equals the reference

value shown in (2.5.9).

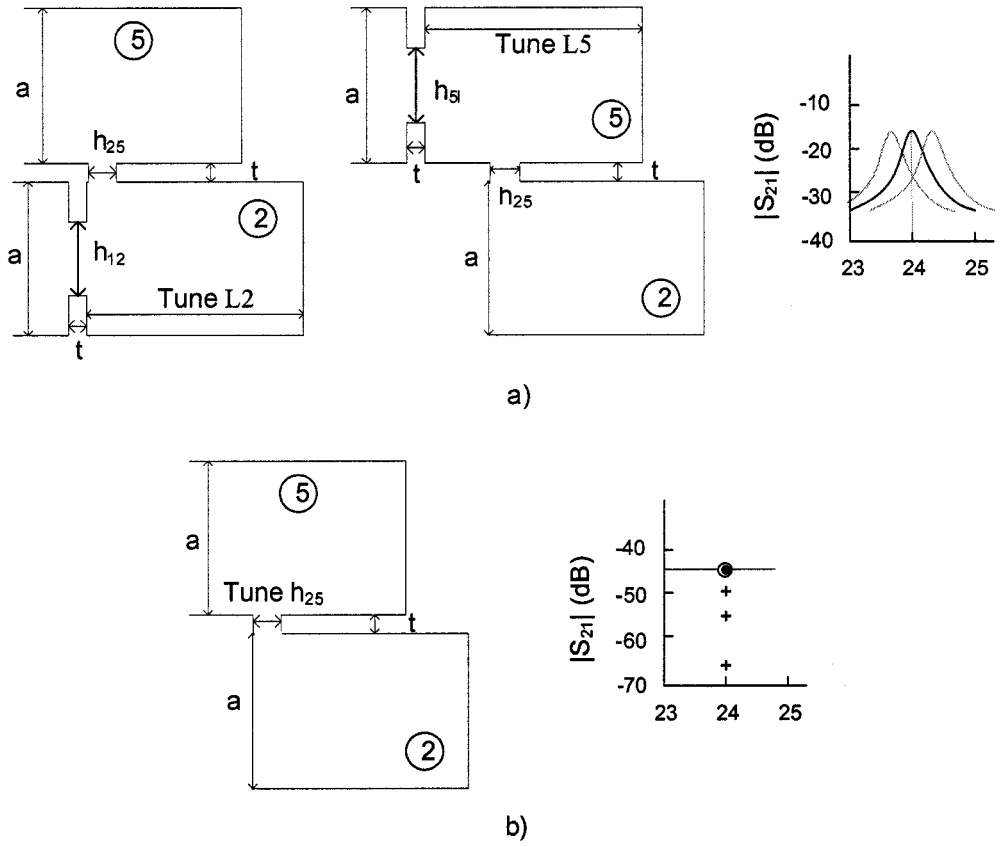

Figure 2- 12: Step 2: a) Length tuning of cavities 2 and 5 for the purpose of b) h_{25} tuning

Step 3, calculate the theoretical $|S_{21}|$ for the coupling between resonators 2 and 5 using equation (1.5.7) with $M_{23} = M_{34} = M_{45} = 0$. Simulate the structure shown in figure 2-13 at 24GHz with the cavity lengths of cavities 2 and 5 found in Step 2, and change the slot width between cavities 2 and 5 until the simulated $|S_{21}|$ equals the above-calculated reference value. This gives a final approximation for the physical dimension h_{25} of the cross-coupling slot between cavities 2 and 5.

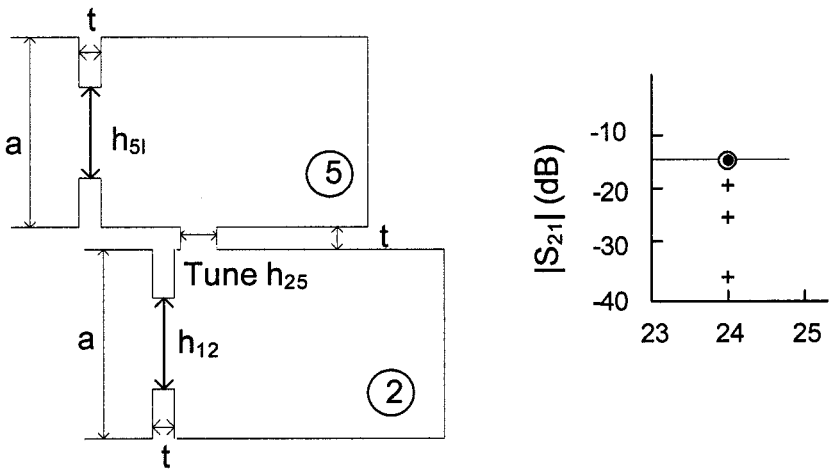

Figure 2- 13: Step3 for the final h_{25} tuning.

Step 4, simulate the 4-port structure in figure 2-14. For $|S_{21}|$, this results in a curve with a single peak at the resonant frequency of the cavity. Adjusting the length of cavities 2 and 5 until the peak is at 24GHz.

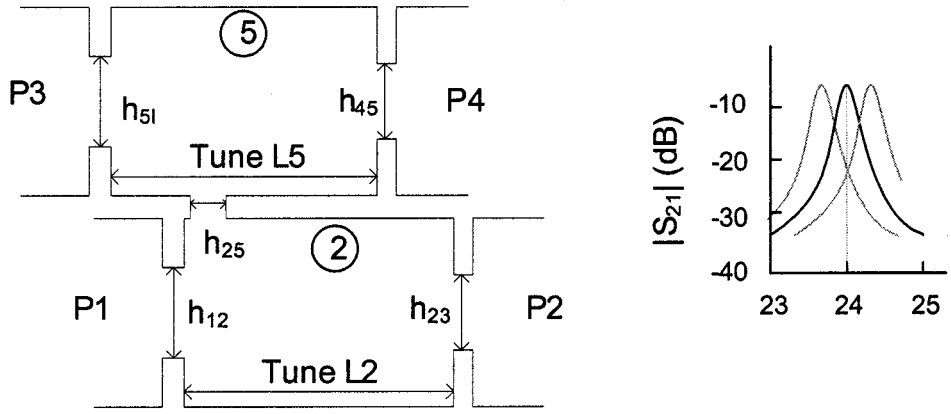

Figure 2- 14: Step 4 for the final length tuning of cavities 2 and 5.

Following steps 1 to 4, the physical dimensions of the cross-coupled SIW cavity filter are finally tuned as:

$$
\begin{aligned}
&h_{s1} = h_{5l} = 63.7mil, h_{12} = 42.3mil, h_{45} = 42.7mil \\
&h_{23} = 38mil, \quad h_{34} = 51.9mil, \quad h_{25} = 23.1mil \\
&l_1 = 173.3mil, \quad l_2 = 182.9mil, \quad l_3 = 185.2mil \\
&l_4 = 184.1mil, \quad l_5 = 173.3mil, \quad t = 12mil
\end{aligned}
\tag{2.6.1}
$$

With this newly obtained set of parameters, we simulate the complete filter again with HFSS, the scattering parameter responses are generated in Figure 2- 15.

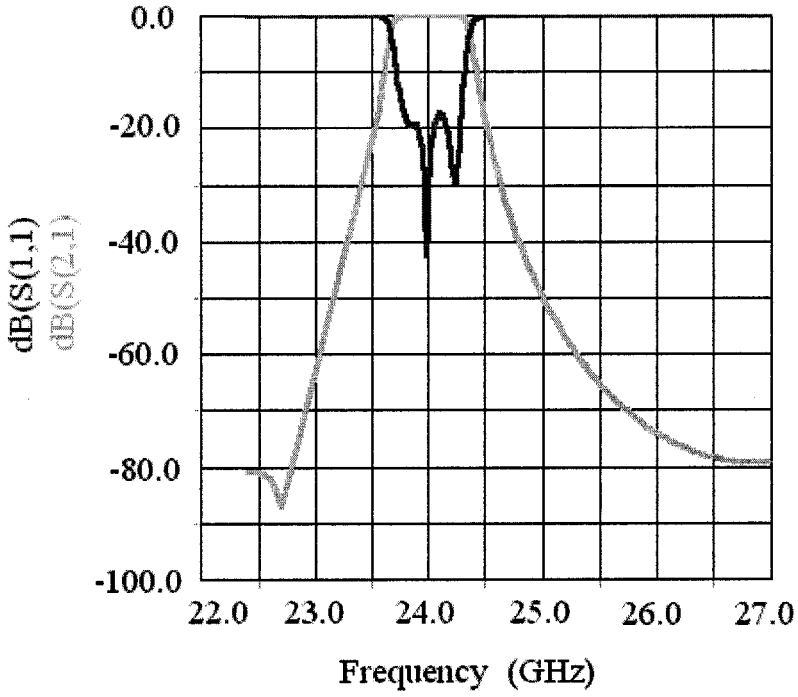

Figure 2- 15: S11 and S21 responses after tuning

Comparing Figure 2- 10 and Figure 2- 15, we can see that after tuning the in-band response shows a great improvement, and the stop-band response has also been improved a little bit. However, the edge response of the pass-band still does not work

well, meaning that the equal-rippled bandwidth is narrowed by about 100MHz than the desired one. From the above phenomenon, we can conclude that, for the symmetrical cross-coupled waveguide filter structure, the tuning method relying on the single-mode circuit model based on a synthesized symmetrical coupling coefficient matrix described in the above may be very useful and efficient [23]. But for the asymmetrical cross-coupled high-order filter structure, for example, in our case, the closely-spaced slots make couplings stronger, complicated and also sensitive. Furthermore, the more the transmission zeros are far away from the pass-band, the more difficult to realize symmetry in both the lower- and the upper-side of the stopband, this has been verified by our simulations and also concluded in reference [24].

Then, it can be proposed that for the asymmetrical cross-coupled high-order filter structures, there are two ways that may be adopted to implement tuning-free design. One is to extract multimode equivalent circuits during the coupling coefficients synthesis process. The other is to use an electromagnetic field analysis-based optimization technique to achieve a global optimization involving all the physical variables based on the initial values that come from a synthesized single-mode based coupling coefficients matrix.

In our work, the global physical variables optimization method is preferred. A mode-matching technique based commercial package called *μWave* Wizard is then

used for achieving our goal. Based on the tuning results in (2.5.11), it is a quite time-saving process with *μWave* Wizard to do the optimization with more than seventeen global variables to be optimized at the same time. Note that the positions of the two cross-coupled irises between cavities 3 and 4, as well as 2 and 5 can make difference with reference to the resulted transmission coefficient responses; they also have to be considered as optimized variables. The schematics of the optimization procedure are shown in Figure 2- 16.

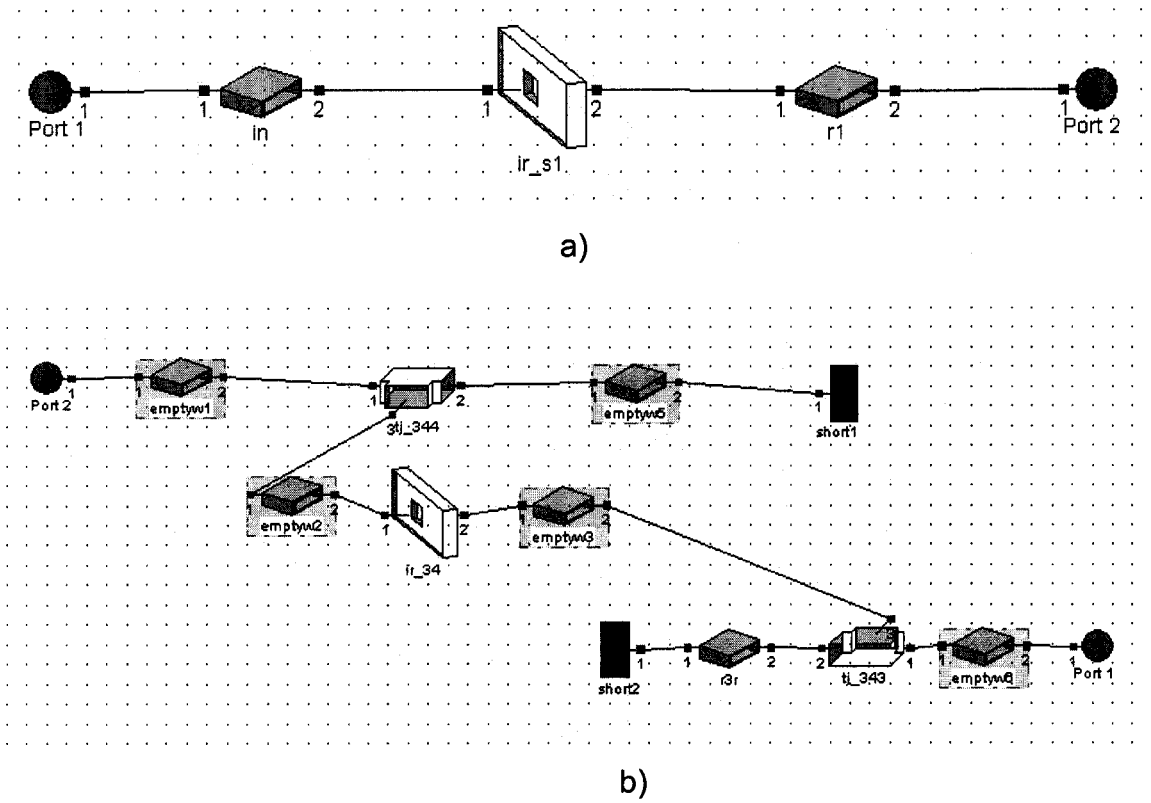

Figure 2-16: Schematics of *μWave* Wizard optimization procedures: a) broad-wall coupling iris sub-circuit; b) cavities 3 and 4 coupling iris sub-circuit.

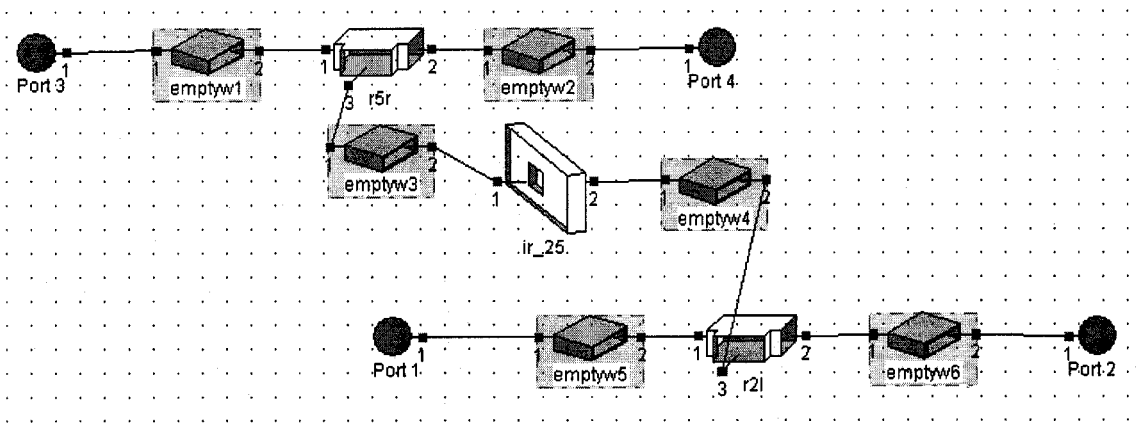

c)

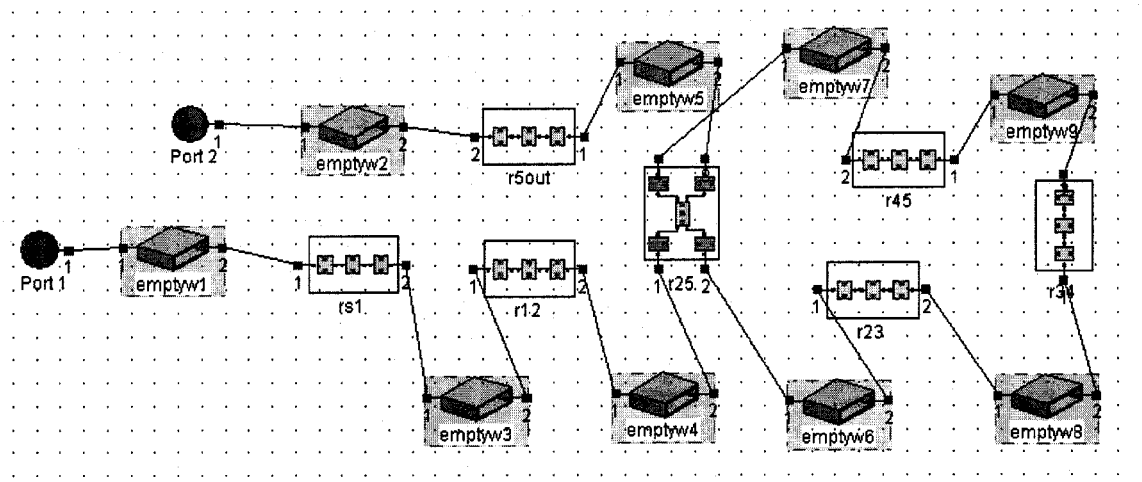

d)

Figure 2- 16: Schematics of *μWave* Wizard optimization procedures: c) cavities 2 and 5 coupling iris sub-circuit and d) the main circuit of filter structure (continued).

A converged optimization result is shown in Figure 2-17. It can be observed that after optimization an in-band return loss of $A_{e\min} \geq 17dB$ is achieved with the desired 3% bandwidth fulfilled, also the stop-band performance is realized by $A_{\min} \geq 60dB$

with two TZs in both sides respectively. The final optimized dimensions are listed in (2.5.12). Compared values in (2.5.12) with those in (2.5.11), it can be found that due to the asymmetrical cross-coupling structure, the realistic coupling matrix is no longer symmetrical. The most critical element is the width of the cross coupling slot between cavities 2 and 5, in order to accomplish the two TZs, it has to be broaden a lot to compensate the interaction from the other closely spaced couplings.

$$
\begin{aligned}
&h_{s1} = 63.3mil,\ h_{5l} = 66.7mil,\ h_{12} = 43.5mil \\
&h_{45} = 44.5mil,\ t = 8.8mil,\ t_{25} = t_{34} = 8.5mil \\
&h_{23} = 40.6mil,\ h_{34} = 55.7mil,\ h_{25} = 34.7mil \\
&l_1 = 173mil,\ l_2 = 181.3mil,\ l_3 = 184.1mil \\
&l_4 = 182.4mil,\ \ l_5 = 170.6mil
\end{aligned}
\qquad (2.6.2)
$$

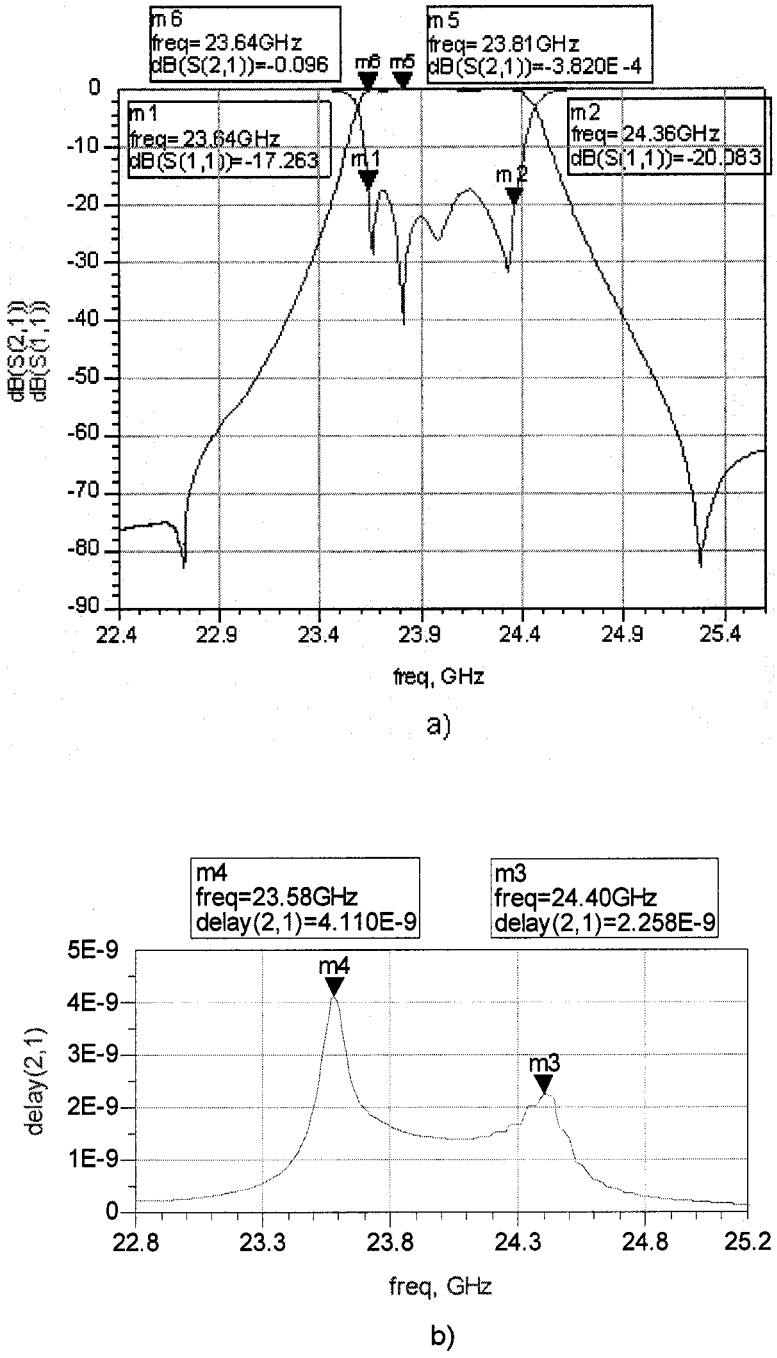

Figure 2- 17: Optimized responses with μWave Wizard : a) insertion and return losses and b) group delay.

We have made the frequency sweeping in a 50% bandwidth to see the stopband performance. From Figure 2-18 it can be seen that from 18GHz to 27.6GHz, the stopband insertion losses are all below -60dB. Around 29.5GHz, the insertion loss is increased but still below -30dB because of the emergence of the TE_{201} resonant mode. Figure 2-19 shows the simulated electrical field distribution at 24GHz.

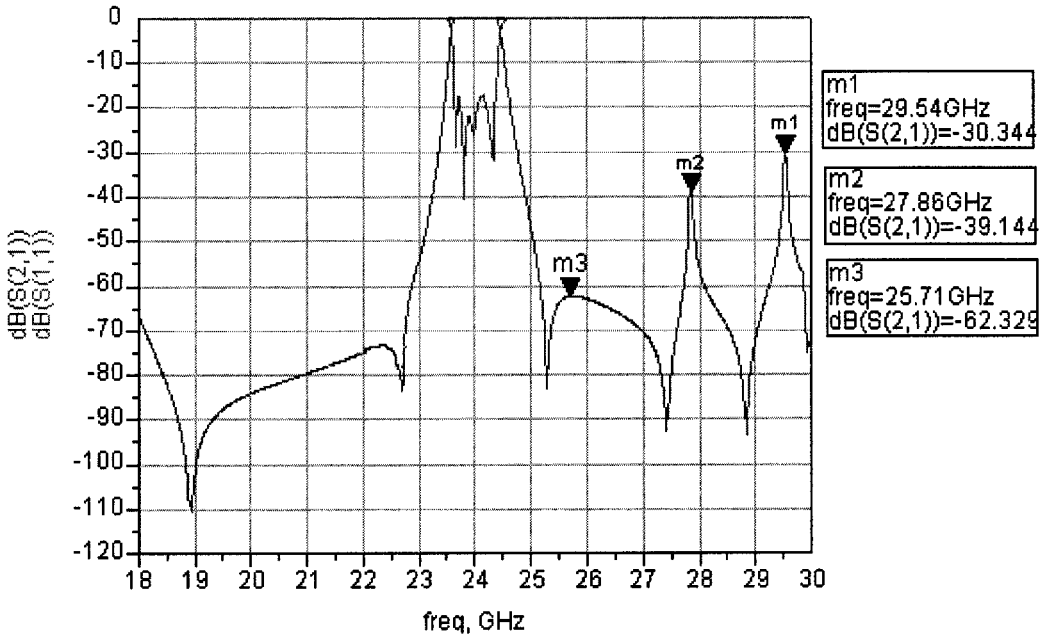

Figure 2- 18: 50% bandwidth sweeping to manifest the stopband performance.

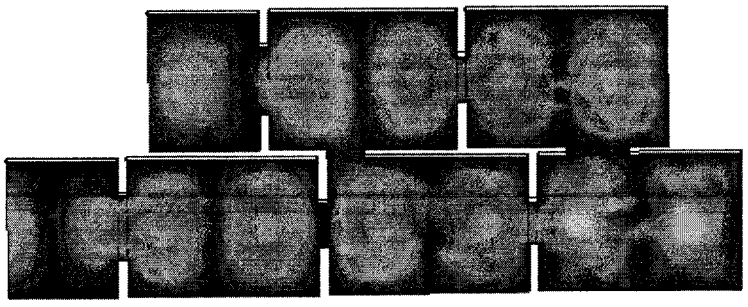

Figure 2- 19: The electrical field distribution at 24GHz.

2.7. Conclusion

From the above synthesis and analysis techniques, it can be understood that due to the frequency-independent single-mode characteristic of the coupling matrix M, it can only give us an approximate evaluation for the inter-cavity couplings. The physical dimensions calculated on the basis of the coupling matrix then give us only an approximate design with a poor return loss response. For structures with not only direct-coupling but also cross-coupling sections, higher-order mode influence turns out to be not negligible because of a much stronger interaction among coupling sections, and a tuning process is necessary for a desired response. In this work, a rapid and useful tuning method has been developed on the method proposed by Jan and Kjetil with some modification for those symmetrical structure waveguide cavity filters with one or more cross couplings. For those asymmetrical high-order filters with several cross couplings, , more tuning efforts need to be done due to very closely placed couplings that make the coupling interactions even stronger and complicated, and a mode-matching technique based global optimization process has successfully been implemented.

Chapter 3. MICROSTRIP TRANSITION DESIGN

3.1. Objective

In order to perform our measurements, a transition between SIW and microstrip is needed. This particular transition was first developed by Dominic [2] as shown in Figure 3- 1, and the advantage of having a large bandwidth is clearly spelled out for this kind of transition.

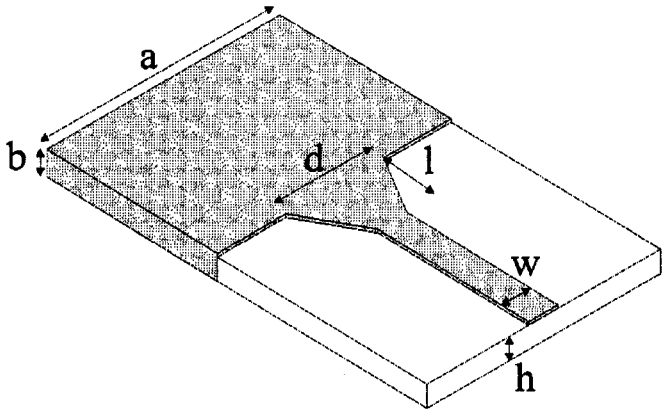

Figure 3- 1:Transition of microstrip line to rectangular waveguide on the same substrate. Source: [2].

3.2. Transition design

For a thickness of h=10mil substrate, 50 Ω microstrip line has a width w=9.6mil. The transition design begins with optimizing the structure which consists of a tapered

microstrip line section connected with a 50 Ω microstrip line on one side and an SIW section on the other side as shown in Figure 3- 1. The optimization process was executed with HFSS simulator by changing the length "*l*" and width "d" till a much better result is reached. With the value of *l*=61mil and d=37mil, an insertion loss better than -0.12 dB and a return loss less than -25dB in the passband are obtained as shown in Figure 3- 2.

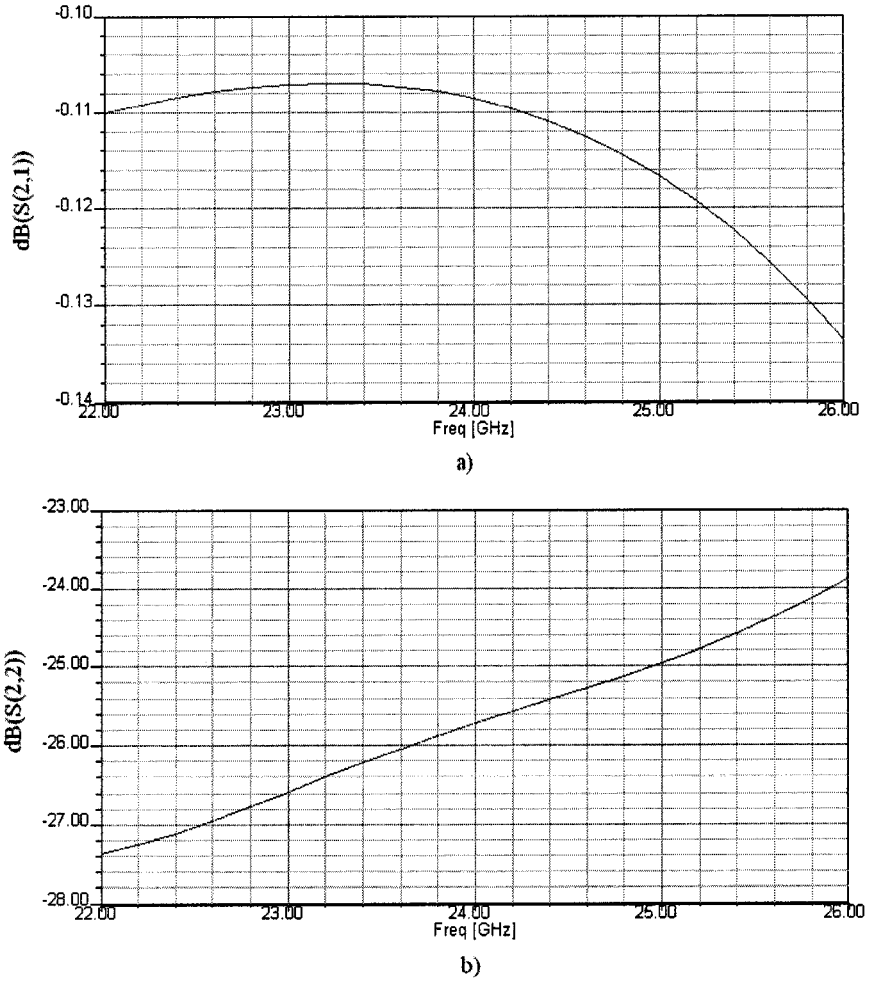

Figure 3- 2: Simulated results for tapered microstrip line to SIW transition: a) Insertion loss and b) Return loss.

Due to the special arrangement that the input and output are on the same side of the

structure, required for measurement, a bend section is considered in the transition design. Between the taper and the microstrip line, we insert a 90° bend section as shown in Figure 3- 3. Let us fix the taper size to be the above optimized value, and also fix the length of the microstrip line to be 160mil, the radius "r" of the bend (the central radium) is then optimized. Finally, a value of r=70mil gives a very good result of insertion loss better than -0.03dB and the return loss less than -30dB in the passband as shown in Figure 3- 4.

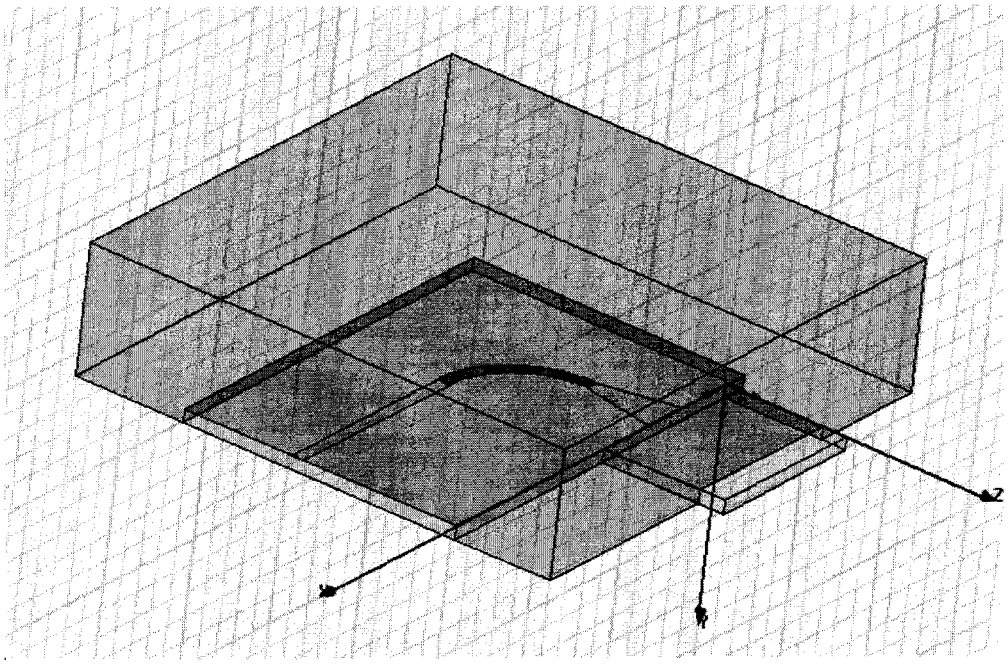

Figure 3- 3: Transition structure to be optimized with HFSS.

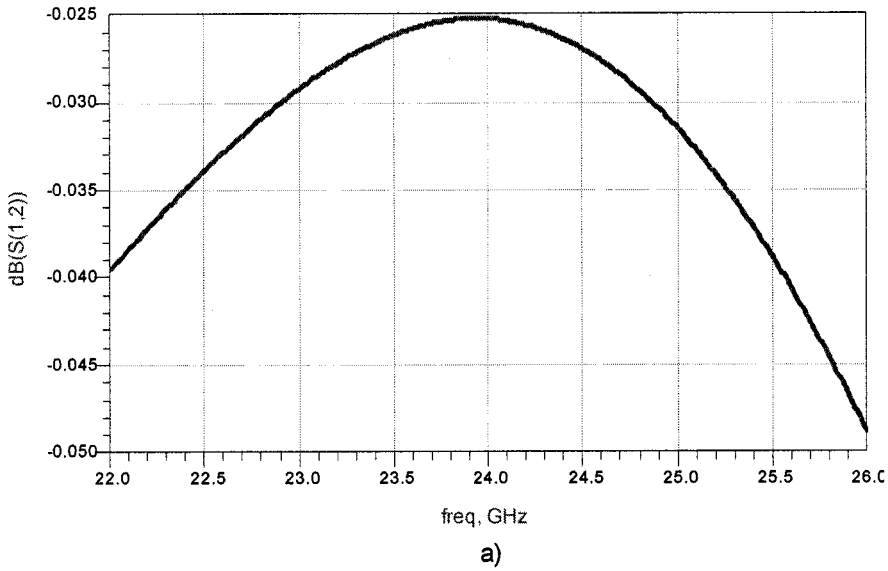

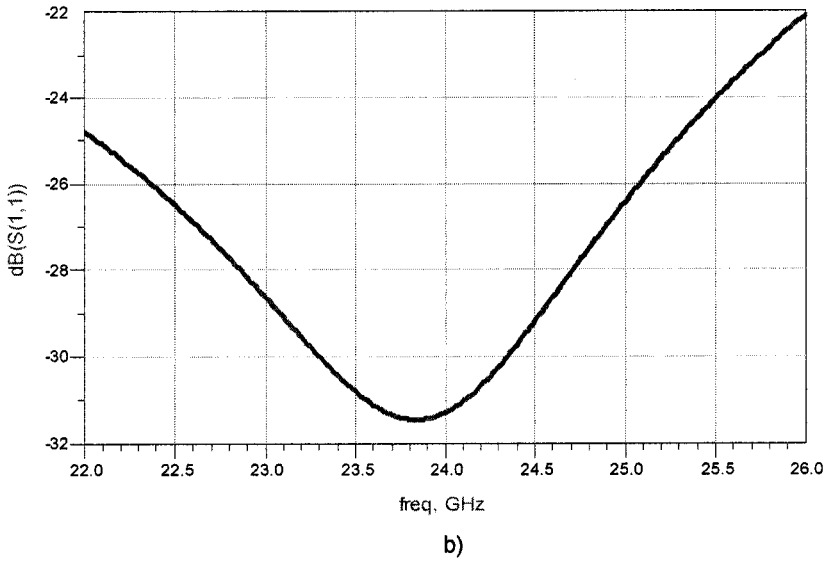

Figure 3- 4: Simulated results for the whole transition design: a) Insertion loss and b) Return loss.

Connecting the transition structure with the SIW filter and taking both dielectric and metallic losses into account, we conduct the simulation again with HFSS to verify whether the transition design can maintain the filter performance, which will give us a prediction of the final overall responses of the designed filter. The results are shown in Figure 3-5, and we can observe that compared Figure 3-5a) with Figure 2-16, the in-band return loss remains good. Due to a low quality factor Q plus the loss from the microstrip transition, nevertheless, the insertion loss at the center frequency of 24.03GHz is increased to -3.615dB. To improve the in-band insertion response characteristic as shown in Chapter 2, more investigations using different substrate materials with different thickness are required. Comparing the broadband sweeping responses in Figure 3-5c) with those in Figure 2-17, we can see that the stop-band performance can not be kept authentically because of the open microstrip transition structure, and this restricts its application of SIW filters to those who do not require an extremely high rejection in the broad stop-band, say below -40dB.

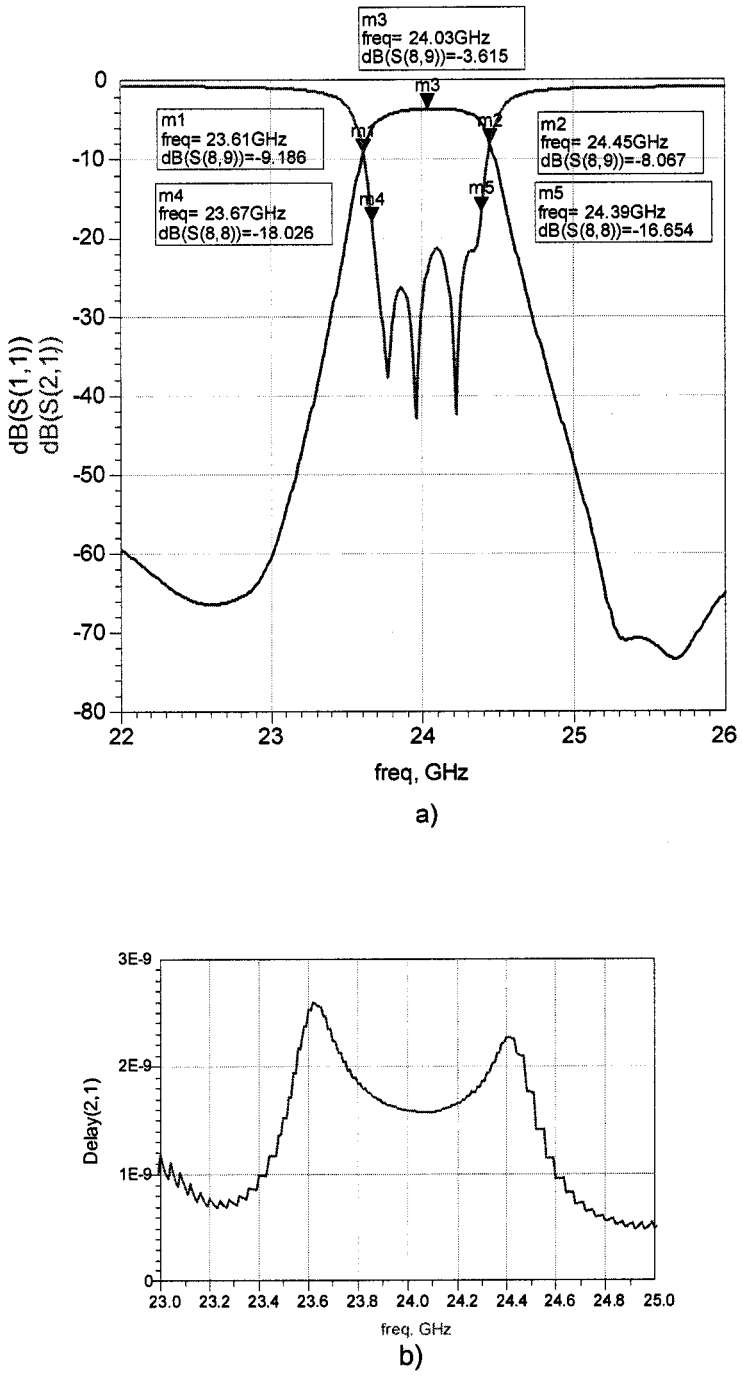

Figure 3- 5: Simulation results with the complete structure of The SIW filter connected with its microstrip transition: a) Insertion and return loss; b) Group delay.

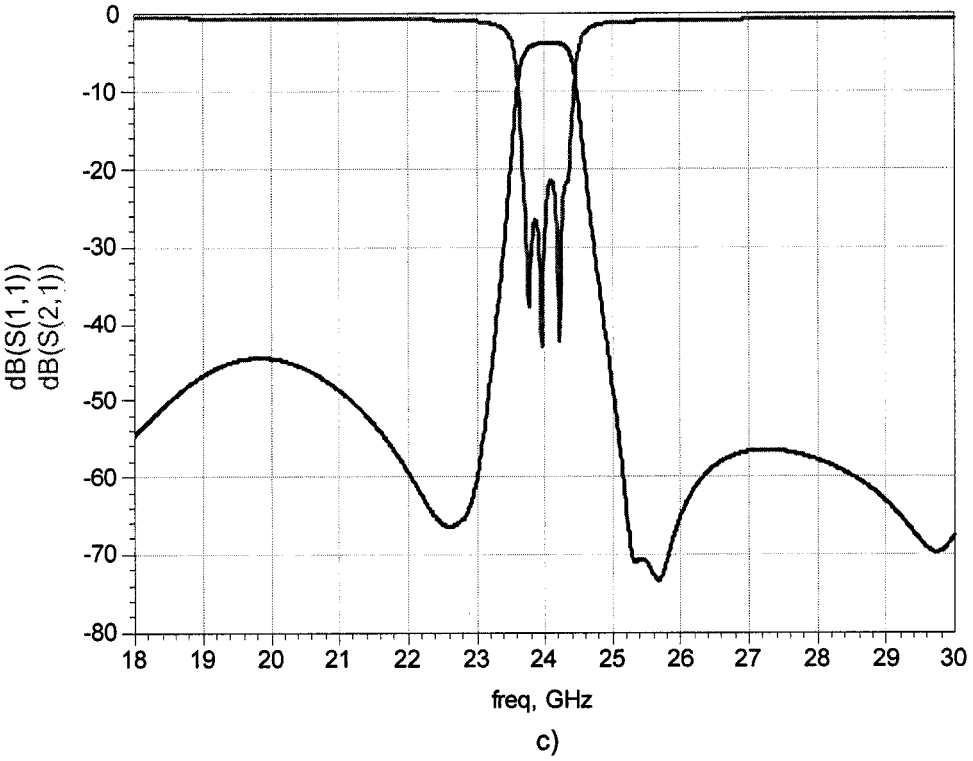

Figure 3- 5: Simulation results with the complete structure of The SIW filter connected with its microstrip transition: c) 50% bandwidth sweep to show the broad stopband performance (continued).

Now, the design process has been completed with a satisfactory result, the research will go into its final part in connection with the fabrication and measurements for experimental verifications.

Chapter 4. FABRICATION AND MEASUREMENTS

4.1. Fabrication

As demonstrated in Chapter 2, the metallized grooves will be used to realize the SIW cavity. In order to guarantee a good mechanic strength of the cavities, a very small-sized connecting strips are designed in the middle of side-walls or at the edge of the broad-wall of cavities. Considering the TE_{102} resonant mode, we know that this gives no influence on the overall filter responses but a very small increase in insertion loss, say less than 0.1dB based on the simulation, which can be ignored in the design. The prototype fabrication was made with a laser micro-maching in our research center, an expected tolerance of $\pm 1mil$ was pre-accounted into the dimension design, then a final precision within $\pm 0.5mil$ can be achieved. The completed prototype is shown in Figure 4- 1.

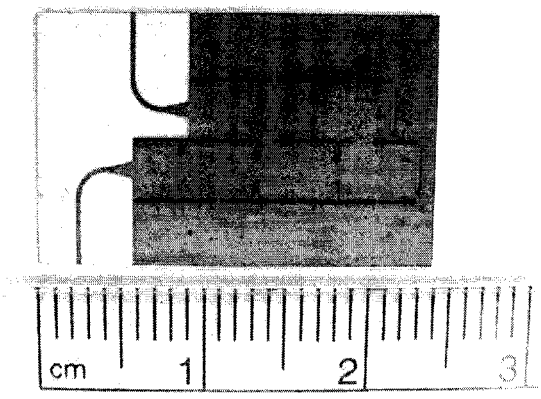

Figure 4- 1: Fabricated 5-degree SIW cavity pseudo elliptic response filter.

4.2. Measurements

4.2.1. TRL calibration design and measurements under the room temperature

The HP 8510 network analyzer was used to perform measurements of the circuit. Because the characteristic impedance of the input and output microstrip line is 50Ω, we used a set of standard 50Ω coaxial calibration kits to perform the measurements. The measured insertion and return loss responses are shown in Figure 4-2.

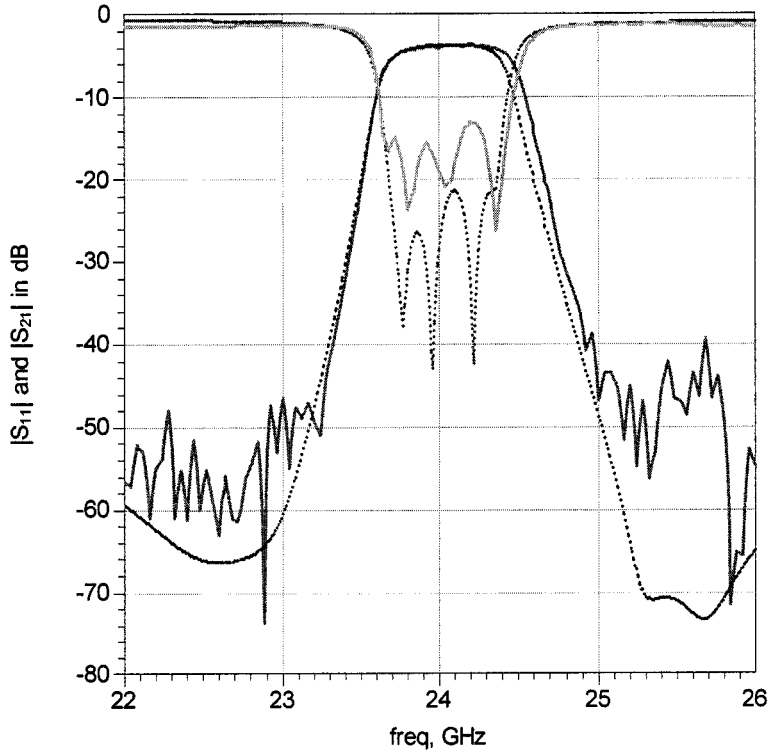

Figure 4- 2: Insertion and return loss: Dot line: Simulated; Solid line: Measured.

Comparing the simulated and measured return loss responses shown in Figure 4-2, we can understand that the calibration taken by choosing coaxial connection planes connecting the network analyzer with the test fixture as the reference planes increases the measured input and output reflection level, it can not give us an authentic record for the filter responses. In order to make error-corrected measurements in non-coaxial transmission media in our case, we should move the reference planes from the coaxial connection planes to the input and output microstrip transmission planes of our filter circuit. Then, a TRL calibration method needs to be taken. This calibration technique is based on a THRU-REFLECT-LINE method, as described in [25]. A non-zero-length THRU is used but specified to have zero delay, the reference plane will be established in the middle of the THRU. The length difference between THRU and LINE has to be $1/4$ wavelength or 90 degrees of insertion phase in the middle of the desired frequency span. However, the insertion phase of the $1/4$ wavelength LINE will vary with frequency, within the frequency span, that is to say, from the start frequency f_1 to the stop frequency f_2, the insertion phase difference between the THRU and LINE must be between 20 and 160 degrees.

On the basis of the above-described principles, the lengths of the THRU, OPEN and LINE were calculated by:

- THRU = 220 mil
- OPEN = 110 mil

- LINE = 266.75 mil

After the TRL calibration, we have carried out measurements again; the obtained scattering parameter responses are shown in Figure 4-3 and Figure 4-4. From Figure 4-3, it can be observed that the measured responses have a good agreement with the simulated ones, and the in-band return loss yields a very good performance of less than -18.45dB, the insertion loss at the center frequency is -3.586dB. Also it can be seen that the measured bandwidth has a 60MHz increasing, and the center frequency is moved to 24.06GHz. All the phenomena suggest that the quality factor Q of our prototype is a little bit higher than the simulated one, which should be attributed to the changes in dielectric permittivity and loss tangent that are defined under the 1MHz frequency condition as shown in Table 2-1. In Figure 4-4, a broadband frequency sweeping response is presented, from which it can be observed that the stopband rejection could be less than -35dB over the whole 50% bandwidth range.

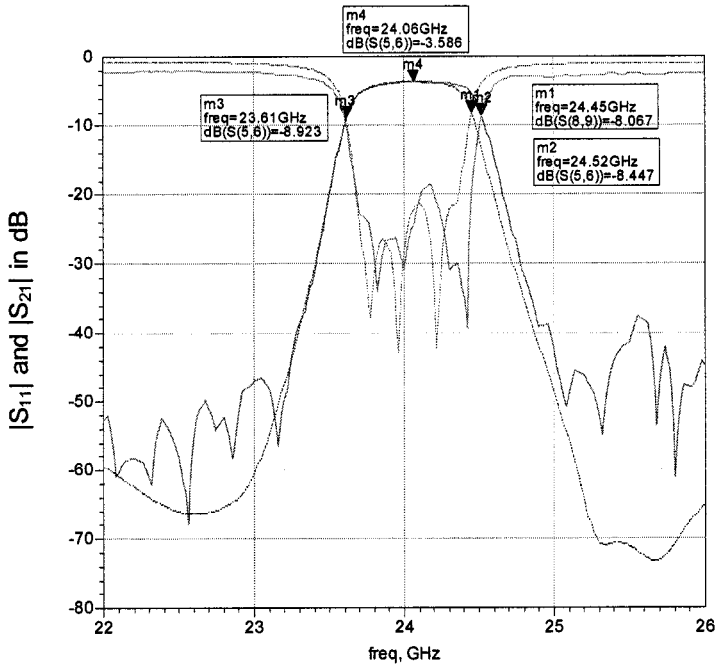

Figure 4- 3: Insertion and return loss: Dot line: Simulated; Solid line: Measured by performing TRL calibration.

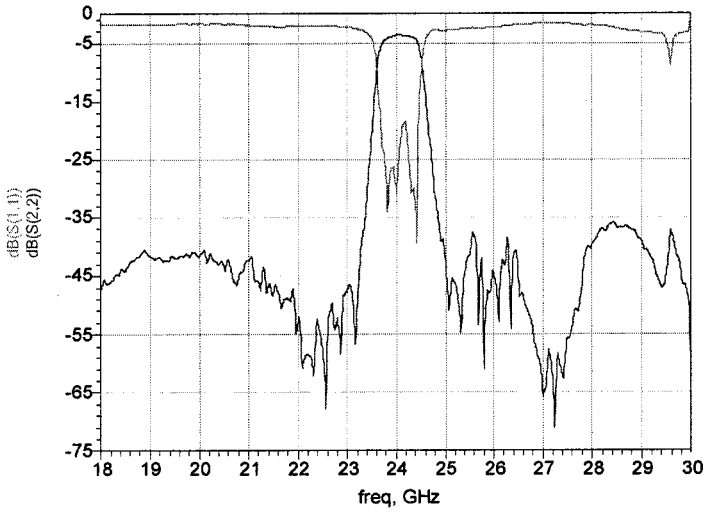

Figure 4- 4: The measured responses over a 50% sweeping bandwidth.

4.2.2. Measurements under different thermal conditions

In some cases, the filter temperature performance is an essential aspect needed for consideration. Temperature is a key factor for the frequency drift, since it affects the coefficient of thermal expansion and the thermal coefficient of the material. The frequency instability with temperature also results from the inherent temperature sensitivity of the dielectric material. The cavity resonator itself is a major cause of the frequency drift with temperature. As temperature varies, the cavity dimension changes, and so does its resonant frequency. Increase in temperature inflates the cavity size then lowers its resonant frequency. In the following, we will evaluate the frequency-temperature performance of our SIW cavity filter by taking a series of measurements under different thermal conditions. The measurements were performed by installing our filter with the test fixture into the Temperature Chamber TEST EQUITY 105, then through its connection insulated holes, the Test Fixture will be connected with the Network Analyzer by coaxial cables as shown in Figure 4-5.

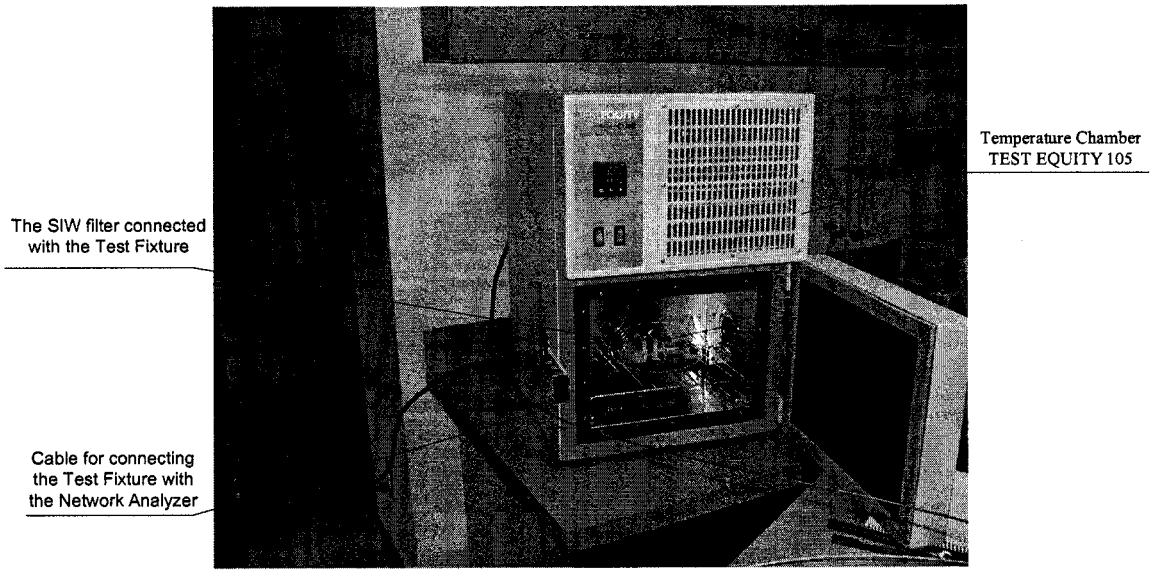

a)

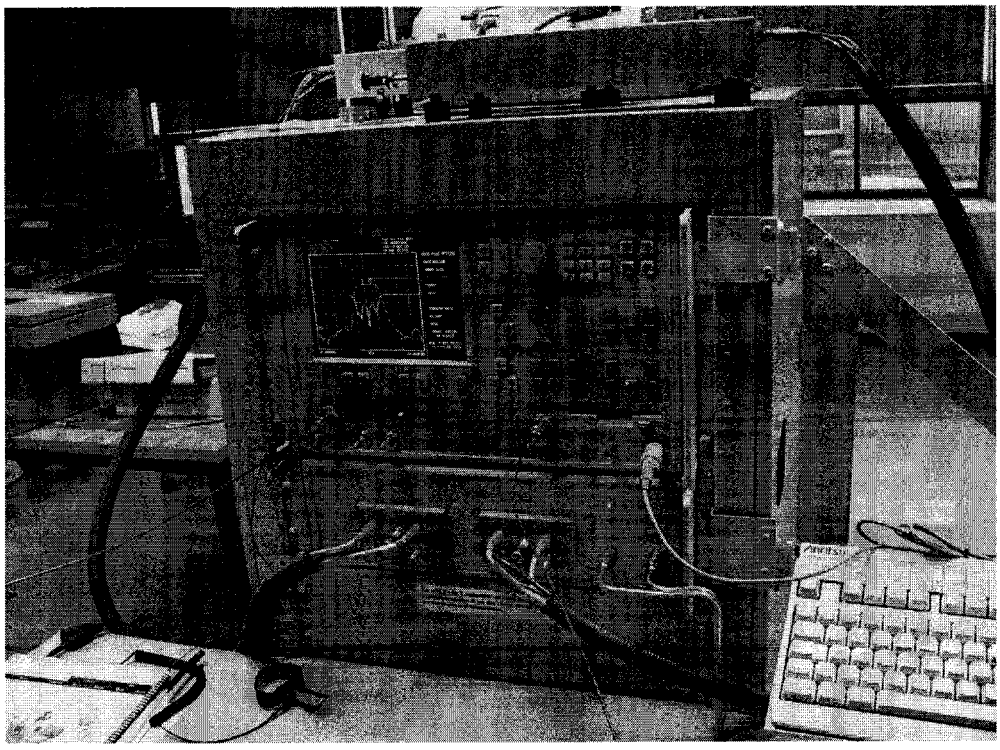

b)

Figure 4- 5: Temperature performance measurement setup: a) The Temperature Chamber and b) The Network Analyzer.

Several sample tests with interval temperature were conducted by setting up two profiles in the Temperature Chamber TEST EQUITY 105 to obtain the temperature behavior of our SIW filter. Table 4-1 gives the tested sample data, and they are also presented in graphic style in Figure 4-6, from which it can be seen that the frequency shift is 115MHz or 0.477% when temperature varies from $-35°c$ to $60°c$. To give a better visualization, the scattering parameter responses at the two extreme temperature points $-35°c$ and $60°c$ are presented in Figure 4-7.

Temperature	Center Frequency (GHz)	Frequency shift compared with that tested under room temperature (MHz)
-35°C	24.16	70
-25°C	24.14	50
-10°C	24.13	40
0°C	24.11	20
11°C	24.095	5
26°C (Room temperature)	24.09	0
40°C	24.085	-5
50°C	24.065	-25
60°C	24.045	-45

Table 4- 1: The tested temperature sample data of the SIW filter.

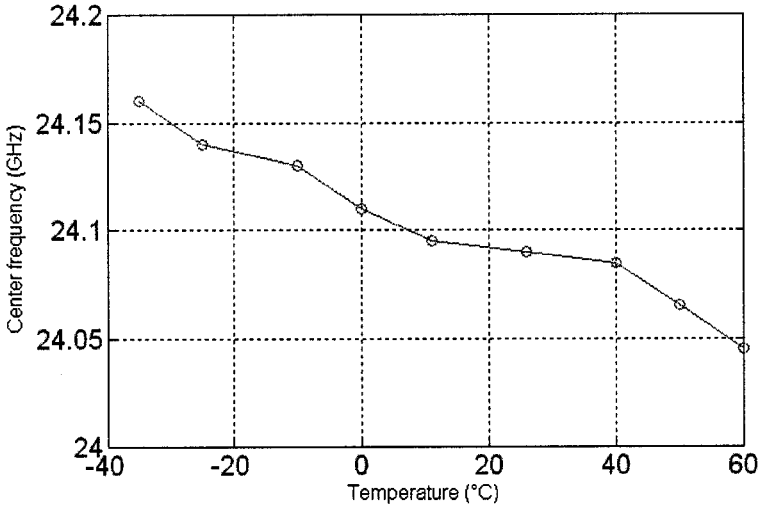

Figure 4- 6: Frequency shift performance of the SIW filter with the temperature variation.

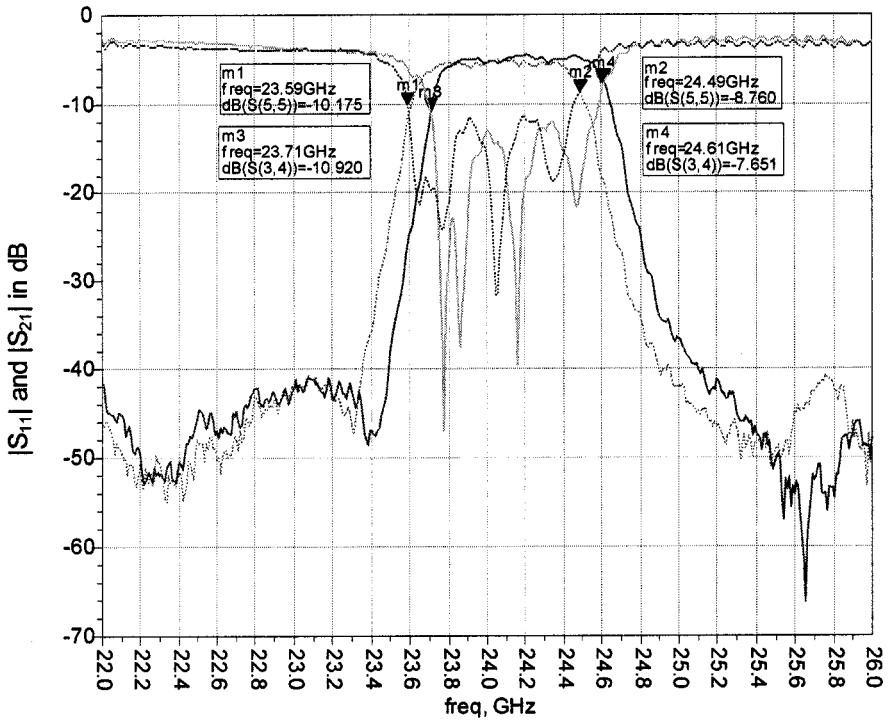

Figure 4- 7: Insertion and return losses measured by performing standard 50Ω kit calibration: Dot line: at temperature of $60°c$; Solid line: at temperature of $-35°c$.

To calculate the frequency-temperature performance of our filter, the following equation should be applied:

$$ppm/^{\circ}C = \frac{1}{\Delta T}\left(\frac{f_1 - f_2}{\frac{f_1 + f_2}{2}}\right) * 10^6 \qquad (4.2.1)$$

Where, ΔT is 95°C, and f_1 and f_2 are frequencies at the extreme temperatures.

Therefore, in our case the frequency-temperature performance is:

$$ppm/^{\circ}C = \frac{1}{95^{\circ}C}\left(\frac{24.16GHz - 24.045GHz}{\frac{24.16GHz + 24.045GHz}{2}}\right) * 10^6 \qquad (4.2.2)$$

$$ppm/^{\circ}C = 50.224$$

Our fabrications and measurements also suggest that the metallization thickness contributes to the insertion loss as well as the frequency-temperature performance of the SIW filter. An increase in metallization thickness tends to worsen the frequency-temperature performance, but to improve the insertion loss characteristics. This requires a substantial research in the future.

CONCLUSIONS AND FUTURE WORK

In this dissertation, a substrate integrated waveguide (SIW) cross-coupled resonant cavity band-pass filter with pseudo-elliptic response is designed and fabricated.

Using the metallized groove scheme which is processed by precision laser machining and our developed metallization technique, a tuning-free substrate integrated waveguide filter has been demonstrated. This pseudo-elliptic function SIW cavity filter presents a fully integrated feature with TE_{10n} / TE_{n01} mode cavity transformation properties which has been verified for SIW manufacturing requirements. Our research indicates that it is pretty straightforward to realize high order filters with high selectivity and finite frequency transmission zeros (TZs). As described in Chapter 1, the coupling structure we adopted in the project restricts its application with a large separation of pass-band TZs. For the realization of near pass-band TZs, the source and load multi-resonator coupling scheme which is also based on TE_{10n} / TE_{n01} mode cavity transformation properties such as example 3 in reference [35] has been confirmed to be useful. The developed SIW cavity filter is a building element in our overall SIW project that are being carried out in our research center. With the present research outcome, some other kinds of SIW filter with different coupling schemes and topologies could be developed in the future.

In this work, a MATLAB code based on an analytical gradient-based optimization technique has been developed and used in the coupling matrix synthesis process, which was confirmed to be an efficient programmable synthesis method, and it can synthesize filters of arbitrary even or odd orders for both symmetric or asymmetric responses. This makes the code useful for other researchers in the future.

A microstrip line to SIW transition has been designed for measurement purpose. From the simulation and measurement results it can be seen that this transition could fulfill the pass-band response but could not precisely give the stop-band response in case that its rejection is less than -40dB. In the future, different types of transitions will be developed to improve the filter response.

In this research, the single-mode circuit model-based coupling matrix synthesis can only give us an initial physical dimension and approximate response of filter, adequate software tuning efforts are needed to get precise dimensions and desired response. In this work, an innovative tuning method has been developed that shows efficient for the symmetric structures. For the asymmetric cross-coupling structures, an optimization process is necessary for the tuning-free fabrication. It has been found that the mode matching technique based optimization method is probably the most efficient scheme in waveguide-based filter design. With this technique good agreements have been achieved among our designs, simulations and measurements, which has confirmed its application

potential of SIW filter.

In addition, we have made measurements in different thermal conditions that have yielded frequency-temperature performance of our SIW cavity filter. It has been found that the metallization thickness can have impact on the insertion loss as well as on the frequency-temperature performance of SIW cavity filter, this phenomenon needs to be studied in detail in the future.

Based on our design technique, SIW resonant cavity with much higher quality factor Q should be studied and realized in the future. And also, a pseudo-elliptic response filter with symmetric structure, to name an example, the folded SIW cavity filter with one or more cross-couplings could be developed, which can yield a very high selectivity and near pass-band TZs without compromise. This may be done with a multilayered scheme.

APPENDIX

% Matlab code for M matrix synthesis;

```
% objfungrad.m;
%%%%%%%%%%%%%%%%%%%%%%%%%%%%%%%%%%%%%%%%%%%%%%%%%%%%
% solve Pn(w);
clear all;
N=5; % set the order of filter;
% set 5 TZs positions;
w1=-4;
w2=4;
w3=-100;
w4=100;
w5=200;

p0=1;
syms w;
p1=w-1/w1;
p2=-p0*(1-w/w1)^2*[(1-1/w2^2)/(1-1/w1^2)]^0.5+p1*[w-1/w2+(w-1/w1)*[(1-1/w2^2)/
(1-1/w1^2)]^0.5];
collect(p2);
p3=-p1*(1-w/w2)^2*[(1-1/w3^2)/(1-1/w2^2)]^0.5+p2*[w-1/w3+(w-1/w2)*[(1-1/w3^2)/
(1-1/w2^2)]^0.5];
collect(p3);
```

```
p4=-p2*(1-w/w3)^2*[(1-1/w4^2)/(1-1/w3^2)]^0.5+p3*[w-1/w4+(w-1/w3)*[(1-1/w4^2)/
(1-1/w3^2)]^0.5];
P4=collect(p4);
p5=-p3*(1-w/w4)^2*[(1-1/w5^2)/(1-1/w4^2)]^0.5+p4*[w-1/w5+(w-1/w4)*[(1-1/w5^2)/
(1-1/w4^2)]^0.5];
p5=collect(p5)
D5=(1-w/w1)*(1-w/w2)*(1-w/w3)*(1-w/w4)*(1-w/w5);

% solve equation of P5=0, get points of zero of Fn(w);
f=solve('-1/200+(1/6666*(-3/2000000*16665^(1/2)-31/160000)*44438889^(1/2)+(6199
69/160000+3/100*16665^(1/2))*(1+1/6666*44438889^(1/2)))*w^5+(1/6666*(619969/1
6000000+3/10000*16665^(1/2))*44438889^(1/2)+(619969/160000+3/100*16665^(1/2)
)*(-1/200-1/666600*44438889^(1/2)))*w^4+((-19687/5000-3/100*16665^(1/2))*(1+1/6
666*44438889^(1/2))+1/6666*(-29997/2000000*16665^(1/2)-154961/80000)*4443888
9^(1/2))*w^3+((-19687/5000-3/100*16665^(1/2))*(-1/200-1/666600*44438889^(1/2))+
1/6666*(-19687/500000-3/10000*16665^(1/2))*44438889^(1/2))*w^2+(1/6666*(4999/
5000+3/200*16665^(1/2))*44438889^(1/2)+1+1/6666*44438889^(1/2))*w=0','w');

wz(1)=f(5);
wz(2)=f(3);
wz(3)=f(4);
wz(4)=f(2);
wz(5)=f(1);

% compute S11(wzi) and the derivatives of S11(wzi) to Mpq & R1 respectively;
syms R1 R2;
```

```
r=1;
R2=r*R1;

for n=1:5
      w=wz(n);

      % use M matrix to express S21 and S11;
     R=[R1 0 0 0 0;0 0 0 0 0;0 0 0 0 0;0 0 0 0 0;0 0 0 0 R2];
     W=[1 0 0 0 0;0 1 0 0 0;0 0 1 0 0;0 0 0 1 0;0 0 0 0 1];
     M=sym('[m11 m12 0 m14 0;m12 m22 m23 0 0;0 m23 m33 m34 0;m14 0 m34 m44
m12;0 0 0 m12 m55]');
     A=-j*R+w*W+M;
     B=inv(A);

     S11=1+2*j*R1*B(1,1);

      S11Z(n)=S11;
      ds11zR1(n)=2*j*B(1,1)+2*R1*(B(1,1)*B(1,1)+r*B(N,1)*B(N,1));
      dms11zR1(n)=real(abs(S11Z(n))/S11Z(n)*ds11zR1(n));
      for p=1:5
           for q=1:5

                if M(p,q)==0
                     P(p,q)=0;
                else P(p,q)=1;
                end
```

```
                ds11zM(n,p,q)=-4*j*R1*P(p,q)*B(1,p)*B(q,1);
                dms11zM(n,p,q)=real(abs(S11Z(n))/S11Z(n)*ds11zM(n,p,q));
            end
        end
    end

% poles of Fn(w);
wp(1)=-4;
wp(2)=4;
wp(3)=-100;
wp(4)=100;
wp(5)=200;

% compute S21(wpi) and the derivatives of S21(wpi) to Mpq & R1 respectively;
 for n=1:5
      w=wp(n);

     R=[R1 0 0 0 0;0 0 0 0 0;0 0 0 0 0;0 0 0 0 0;0 0 0 0 R2];
     W=[1 0 0 0 0;0 1 0 0 0;0 0 1 0 0;0 0 0 1 0;0 0 0 0 1];
     M=sym('[m11 m12 0 m14 0;m12 m22 m23 0 0;0 m23 m33 m34 0;m14 0 m34 m44
m12;0 0 0 m12 m55]');
     A=-j*R+w*W+M;
     B=inv(A);

     S21=-2*j*sqrt(R1*R2)*B(N,1);
```

```
        S21p(n)=S21;

ds21pR1(n)=-2*j*sqrt(r)*B(N,1)+2*R1*sqrt(r)*(B(N,1)*B(1,1)+r*B(N,N)*B(N,1));
        dms21pR1(n)=real(abs(S21p(n))/S21p(n)*ds21pR1(n));
        for p=1:5
            for q=1:5
                if M(p,q)==0
                    P(p,q)=0;
                else P(p,q)=1;
                end

ds21pM(n,p,q)=2*j*sqrt(R1*R2)*P(p,q)*(B(N,p)*B(q,1)+B(N,q)*B(p,1));
                dms21pM(n,p,q)=real(abs(S21p(n))/S21p(n)*ds21pM(n,p,q));
            end
        end
 end

% compute S11(w=1,-1) and the derivatives of S11(w=1,-1) to Mpq & R1 respectively;
w(1)=1;
w(2)=-1;
for n=1:2
      w=w(n);
       R=[R1 0 0 0 0;0 0 0 0 0;0 0 0 0 0;0 0 0 0 0;0 0 0 0 R2];
      W=[1 0 0 0 0;0 1 0 0 0;0 0 1 0 0;0 0 0 1 0;0 0 0 0 1];
      M=sym('[m11 m12 0 m14 0;m12 m22 m23 0 0;0 m23 m33 m34 0;m14 0 m34 m44
m12;0 0 0 m12 m55]');
```

```
    A=-j*R+w*W+M;
    B=inv(A);

  S11=1+2*j*B(1,1);

    S11(n)=S11;
    ds11R1(n)=2*j*B(1,1)+2*R1*(B(1,1)*B(1,1)+r*B(N,1)*B(N,1));
    dms11R1(n)=real(abs(S11(n))/S11(n)*ds11R1(n));
     for p=1:5
          for q=1:5
               if M(p,q)==0
                    P(p,q)=0;
               else P(p,q)=1;
               end
               ds11M(n,p,q)=-4*j*R1*P(p,q)*B(1,p)*B(q,1);
               dms11M(n,p,q)=real(abs(S11(n))/S11(n)*ds11M(n,p,q));
          end
     end
 end

% cost function K and its analytical gradient G;
RL=22;
diecons=(10^(RL/10)-1)^(-1/2);
cons=diecons/sqrt(1+diecons^2);

S11Zn=0;
```

```
S21pn=0;
for n=1:5
    S11Zn=S11Zn+abs(S11Z(n))^2;
    S21pn=S21pn+abs(S21p(n))^2;
end

K=S11Zn+S21pn+(abs(S11(2))-cons)^2+(abs(S11(1))-cons)^2;

    for p=1:5
        for q=1:5
            for n=1:5

Gf2(n)=abs(S11Z(n))*dms11zM(n,p,q)+abs(S21p(n))*dms21pM(n,p,q);
            end
            Gf2s(p*q)=Gf2(1)+Gf2(2)+Gf2(3)+Gf2(4)+Gf2(5);
            for n=1:2
            Gr2(n)=abs(S11(n))*dms11M(n,p,q)-cons*ds11M(n,p,q);
            end
            Gr2s(p*q)=Gr2(1)+Gr2(2);
            G(p*q)=2*(Gf2s(p*q)+Gr2s(p*q));
        end
    end

for n=1:5
    GR1f(n)=abs(S11Z(n))*dms11zR1(n)+abs(S21p(n))*dms21pR1(n);
end
```

```
GR1fs=GR1f(1)+GR1f(2)+GR1f(3)+GR1f(4)+GR1f(5);
for n=1:2
    GR1r(n)=abs(S11(n))*dms11R1(n)-cons*ds11R1(n);
end
GR1rs=GR1r(1)+GR1r(2);
G(p*q+1)=2*(GR1fs+GR1rs);

x=[R1 m11 m12 m14 m22 m23 m33 m34 m44 m55];
function[K,G]=objfungrad(x);

%%%%%%%%%%%%%%%%%%%%%%%%%%%%%%%%%%%%%%%%%%%%%%%


% confungrad.m;
%%%%%%%%%%%%%%%%%%%%%%%%%%%%%%%%%%%%%%%%%%%%%%%

function[c,ceq,dc,dceq]=confungrad(x);

c=[x(3)-x(1);x(6)-x(3);x(8)-x(6);x(4)-x(3)];
dc=[-1,0,0,0;0,0,0,0;1,-1,0,-1;0,0,0,1;0,0,0,0;0,1,-1,0;0,0,0,0;0,0,1,0;0,0,0,0;0,0,0,0];

ceq=[];
dceq=[];

%%%%%%%%%%%%%%%%%%%%%%%%%%%%%%%%%%%%%%%%%%%%%%%
```

```
% filsynthesis.m;
%%%%%%%%%%%%%%%%%%%%%%%%%%%%%%%%%%%%%%%%%%%%
% minimize cost function,get solution;

x0=[1 0 0.5 0 0 0.5 0 0.5 0 0];

options=optimset('LargeScale','off');
options=optimset(options,'GradObj','on','GradConstr','on');

[x,fval,exitflag,output]=fmincon('objfungrad',x0,[],[],[],[],[],[],'confungrad',options);

%%%%%%%%%%%%%%%%%%%%%%%%%%%%%%%%%%%%%%%%%%%%
```

REFERENCES

[1] H. Uchimura, T. Takenoshita, M. Fuji, "Development of a Lamined Waveguide", IEEE Trans. Microwave Theory and Techniques, Vol. 46. Dec. 1998, pp. 2438-2443.

[2] D. Deslandes and K. Wu, "Integrated Microstrip and Rectangular Waveguide in Planar Form", IEEE Microwave and wireless Components Letters, Vol. 11 Feb. 2001, pp. 68-70.

[3] U. Rosenberg, "New 'Planar' Waveguide Cavity Elliptic Function Filters", in Proc 25th Eur. Microwave Conf., Bologna, Italy, Sept. 1995, pp.524-527.

[4] R. Saal and E. Ulbrich, "On the Design of Filters by Synthesis", IRE Transactions on Circuit Theory, Dec.1958.

[5] A. J. Pilote, K. A. Leahy, B. A. Flanik, K. A. Zaki, "Waveguide Filters Having a Layered Dielectric Structure", U.A. Patent, No. 5 382 931, Jan 17 1995.

[6] Zverev, Anatol. L, New York, Toronto: John Wiley & Sons Inc., c1967, Handbook of Filter Synthesis, 576p.

[7] A. E. Atia and A. E. Williams, "Narrow-Bandpass Waveguide Filters", IEEE Trans. Microwave Theory Tech., vol. MTT-20, pp. 258–265, Apr. 1972.

[8] A. E. Atia, A. E. Williams, and R. W. Newcomb, "Narrow-Band Multiple-Coupled Cavity Synthesis", IEEE Trans. Circuit Syst., vol. CAS-21, pp. 649–655, Sept. 1974.

[9] R. M. Kurzrok, "General Three-Resonator Filters in Waveguides", IEEE Trans. Microwave Theory Tech., vol. MTT-14, pp. 46–47, Jan. 1966.

[10] R. M. Kurzrok, "General Four-Resonator Filters at Microwave Frequencies", IEEE Trans. Microwave Theory Tech., vol. MTT-14, pp. 295–296, June 1966.

[11] A. E. Williams, "A Four-Cavity Elliptic Waveguide Filter", IEEE Trans. Microwave Theory Tech., vol. MTT-18, pp. 1109–1114, Dec. 1970.

[12] R. J. Cameron and J. D. Rhodes, "Asymmetric Realizations of Dual-Mode Bandpass Filters", IEEE Trans. Microwave Theory Tech., vol. MTT-29, pp. 51–58, Jan. 1981.

[13] D. Chambers and J. D. Rhodes, "A Low Pass Prototype Allowing the Placing of Integrated Poles at Real Frequencies", IEEE Trans. Microwave Theory Tech., vol. MTT-31, pp. 40–45, Jan. 1983.

[14] R. Levy, "Direct Synthesis of Cascaded Quadruplet (CQ) Filters," IEEE Trans. Microwave Theory Tech., vol. 43, pp. 2940–2944, Dec. 1995.

[15] R. Levy, "Filters with Single Transmission Zeros at Real or Imaginary Frequencies", IEEE Trans. Microwave Theory Tech., vol. MTT-24, pp.172–181, April 1976.

[16] G. Pfitzenmaier, "Synthesis and Realization of Narrow-Band Canonical Microwave Bandpass Filters Exhibiting Linear Phase and Transmission Zeros", IEEE Trans. Microwave Theory Tech., vol. MTT-30, pp.1300–1311, Sep. 1982.

[17] W. A. Atia, K. A. Zaki, and A. E. Atia, "Synthesis of General Topology Multiple Coupled Resonator Filters by Optimization", IEEE Microwave Theory Tech. Dig., pp. 821–824, 1998.

[18] R. J. Cameron, "General Coupling Matrix Synthesis Methods for Chebychev Filtering Functions", IEEE Trans. Microwave Theory Tech., vol. 47, pp. 433–442, Apr. 1999.

[19] S. Amari, "Synthesis of Cross-Coupled Resonator Filters Using an Analytical Gradient-Based Optimization Technique", IEEE Trans. Microwave Theory Tech., vol. 48, No. 9, Sep. 2000.

[20] David M. Pozar, 2nd edition, New York, Toronto: John Wiley & Sons Inc., 1998, Microwave Engineering, 716p.

[21] G. Matthaei L. Young and E.M.T. Jones, 1980, Microwave Filters, Impedance-Matching Networks, and Coupling Structures, 1096p.

[22] Hunter, Lan C., London: Institution of Electrical Engineers, c2001, Theory and Design of Microwave Filters, 353p.

[23] J. Kocbach and K. Folgerø, "Design Procedure for Waveguide Filters with Cross-Couplings", Microwave Symposium Digest, 2002 IEEE MTT-S International, volume: 3, 2-7 June 2002.

[24] Levy, R.; Snyder, R.V.; Matthaei, G., "Design of Microwave Filters", IEEE

Transactions, Microwave Theory and Techniques, Volume: 50, Issue: 3, March 2002.

[25] Product Note 8510-8A "Applying the HP 8510 TRL Calibration for Non-Coaxial Measurements" HP.

[26] H. J. Orchard, "Filter Design by Iterated Analysis", IEEE Trans. Circuits Syst., vol. 32, pp. 1089-1096, Nov. 1985.

[27] W. H. Press, B. P. Flannery, S. A. Teukolsky, and W. T. Wetterling, Numerical Recipes, New York, NY: Cambridge Univ. Press, 1986.

[28] Y. Cassivi and K. Wu. "Low-Cost Microwave Oscillator Using SIW Cavity", Submitted to Microwave and Wireless Components Letters, 2002.

[29] Y. Cassivi, L. Perregrini, K. Wu and al., "Dispersion Characteristics of SIW", accepted for publication, IEEE Microwave and Wireless Components Letters, 2002.

[30] Y. Cassivi, D. Deslandes, K. Wu "Substrate Integrated Waveguide Directional Couplers", Asia-Pacific Microwave Conference, 2002.

[31] D. Deslandes and K. Wu "Design Considerations and Performance Analysis of Substrate Integrated Waveguide Components" European Microwave Conference, 23-27 Sept. 2002, pp.881-884.

[32] D. Deslandes and K. Wu, "Single-Substrate Integration Technique of Planar Circuits and Waveguide Filters" IEEE Trans. On Microwave Theory and Techniques, Vol. 51, No. 2, Feb. 2003.

[33] S. Germain, D. Deslandes and K. Wu, "Development of Substrate Integrated Waveguide Power Dividers". CCECE 2003 – CCGEI 2003, Montréal, May 2003.

[34] K. Wu, D. Deslandes, Y. Cassivi, "The Substrate Integrated Circuits - a New Concept for High-Frequency Electronics and Optoelectronics," TELSIKS'03, pp. P-III – P-X, Nis, Yugoslavia, Oct. 1-3, 2003.

[35] Rosenberg, U. and Amari, S., "Novel Coupling Schemes for Microwave Resonator Filters", IEEE Trans. On Microwave Theory and Tech., vol. 50, No. 12, Dec. 2002, pp. 2896- 2902.